

that GMFG may be an attractive new target for pharmacotherapeutic agents to treat such diseases.

### Acknowledgments

We thank Dr Kiyofumi Asai for providing the anti-sera for GMFG. We thank Dr Yoshimi Takai for providing the expression constructs of dominant active and dominant negative Rho, Rac, and Cdc42. We thank Dr Alex Dunn for helpful suggestions for actin-binding and Arp2/3 complex-binding assays.

### Source of Funding

This work was supported by the Donald W. Reynolds Foundation.

### Disclosures

None.

### References

1. Ho M, Yang E, Matcuk G, Deng D, Sampas N, Tsalenko A, Tabibiazar R, Zhang Y, Chen M, Talbi S, Ho YD, Wang J, Tsao PS, Ben-Dor A, Yakhini Z, Bruhn L, Quertermous T. Identification of endothelial cell genes by combined database mining and microarray analysis. *Physiol Genomics*. 2003;13:249–262.
2. Asai K, Fujita K, Yamamoto M, Hotta T, Moriyama M, Kokubo M, Moriyama A, Kato T. Isolation of novel cDNA (hGMF-gamma) homologous to glia maturation factor-beta gene. *Biochim Biophys Acta*. 1998;1396:242–244.
3. Pollard TD, Blanchoin L, Mullins RD. Molecular mechanisms controlling actin filament dynamics in nonmuscle cells. *Annu Rev Biophys Biomol Struct*. 2000;29:545–576.
4. Carlier MF, Ressad F, Pantaloni D. Control of actin dynamics in cell motility. Role of ADF/cofilin. *J Biol Chem*. 1999;274:33827–33830.
5. Yamazaki D, Suetsugu S, Miki H, Kataoka Y, Nishikawa S, Fujiwara T, Yoshida N, Takenawa T. WAVE2 is required for directed cell migration and cardiovascular development. *Nature*. 2003;424:452–456.
6. Bamburg JR, Wiggan OP. ADF/cofilin and actin dynamics in disease. *Trends Cell Biol*. 2002;12:598–605.
7. Zhang J, Shehabeldin A, da Cruz LA, Butler J, Somani AK, McGavin M, Koziaradzki I, dos Santos AO, Nagy A, Grinstein S, Penninger JM. Antigen receptor-induced activation and cytoskeletal rearrangement are impaired in Wiskott-Aldrich syndrome protein-deficient lymphocytes. *J Exp Med*. 1999;190:1329–1342.
8. Goode BL, Drubin DG, Lappalainen P. Regulation of the cortical actin cytoskeleton in budding yeast by twinfilin, a ubiquitous actin monomer-sequestering protein. *J Cell Biol*. 1998;142:723–733.
9. Bamburg JR. Proteins of the ADF/cofilin family: essential regulators of actin dynamics. *Annu Rev Cell Dev Biol*. 1999;15:185–230.
10. Ghosh M, Song X, Mounicimnc G, Sidani M, Lawrence DS, Condeelis JS. Cofilin promotes actin polymerization and defines the direction of cell motility. *Science*. 2004;304:743–746.
11. Hirata KI, Ishida T, Penta K, Rezace M, Yang E, Wohlgenuth J, Quertermous T. Cloning of an immunoglobulin family adhesion molecule selectively expressed by endothelial cells. *J Biol Chem*. 2001;276:16223–16231.
12. Ikeda K, Quertermous T. Molecular isolation and characterization of a soluble isoform of activated leukocyte cell adhesion molecule that modulates endothelial cell function. *J Biol Chem*. 2004;279:55315–55323.
13. Olazabal IM, Machesky LM. Abp1p and cortactin, new “hand-holds” for actin. *J Cell Biol*. 2001;154:679–682.
14. Nian M, Lee P, Khaper N, Liu P. Inflammatory cytokines and postmyocardial infarction remodeling. *Cir Res*. 2004;94:1543–1553.
15. Naldini A, Carraro F. Role of inflammatory mediators in angiogenesis. *Curr Drug Targets Inflamm Allergy*. 2005;4:3–8.
16. Asahara T, Murohara T, Sullivan A, Silver M, van der Zec R, Li T, Witzenbichler B, Schatteman G, Isner JM. Isolation of putative progenitor endothelial cells for angiogenesis. *Science*. 1997;275:964–967.
17. Salven P, Mustjoki S, Alitalo R, Alitalo K, Rafii S. VEGFR-3 and CD133 identify a population of CD34+ lymphatic/vascular endothelial precursor cells. *Blood*. 2003;101:168–172.



ELSEVIER

Available online at [www.sciencedirect.com](http://www.sciencedirect.com)

SCIENCE @ DIRECT®

Journal of Molecular and Cellular Cardiology 40 (2006) 799–809

Journal of  
Molecular and  
Cellular Cardiology

[www.elsevier.com/locate/yjmcc](http://www.elsevier.com/locate/yjmcc)

Original article

## Myocardium-targeted delivery of endothelial progenitor cells by ultrasound-mediated microbubble destruction improves cardiac function via an angiogenic response

Kan Zen<sup>a</sup>, Mitsuhiro Okigaki<sup>a,\*</sup>, Yohei Hosokawa<sup>b</sup>, Yasushi Adachi<sup>c</sup>, Yoshihisa Nozawa<sup>d</sup>,  
Michitaka Takamiya<sup>a</sup>, Tetsuya Tatsumi<sup>a</sup>, Norifumi Urao<sup>a</sup>, Kento Tateishi<sup>a</sup>,  
Tomosaburo Takahashi<sup>a</sup>, Hiroaki Matsubara<sup>a</sup>

<sup>a</sup> Department of Cardiovascular Medicine, Kyoto Prefectural University of Medicine, Kamigyo-ku, Kyoto, 602-8566, Japan

<sup>b</sup> Department of Pathology, Omihachiman City Hospital, Japan

<sup>c</sup> First Department of Pathology, Kansai Medical University, Japan

<sup>d</sup> Pharmacobioregulation Research Laboratory, Taiho Pharmaceutical Co. Ltd, Suitama, Japan

Received 24 January 2006; accepted 14 March 2006

Available online 5 May 2006

### Abstract

Application of ultrasound-mediated destruction of microbubbles (US + Bubble) to skeletal muscle creates capillary ruptures leading to leakage of the cell components. We studied whether US + Bubble combined with bone-marrow-derived mononuclear cells (BM-MNCs) infusion enables the targeted delivery of endothelial-lineage cells into the myocardium and improves cardiac function of the cardiomyopathy model due to the paucity of neocapillary formation. Pulsed US was applied to the anterior chest of BIOTO2 cardiomyopathy hamsters for 90 s after the intravenous injection of microbubble (Optison<sup>®</sup>) followed by infusion of BM-MNCs. Cardiac samples from US + microbubble + BM-MNCs (US + Bubble + BM), US + Bubble, US + BM without Bubble, and saline infusion control groups were analyzed 12 weeks after treatment. Labeled BM-MNCs transplanted by US + Bubble were found to be mainly localized in the microvessels, but not by US stimulation without microbubble ( $121.2 \pm 24.5$  vs.  $2.80 \pm 1.30$  cells/mm<sup>2</sup>,  $P < 0.001$ ). Capillary densities in US + Bubble + BM group were increased 1.7-fold ( $P < 0.05$ ) over the control, and neither US + Bubble nor US + BM enhanced neocapillary formation. <sup>99m</sup>Tc-Tetrofosmin scintigraphy revealed that blood perfusion area in the US + Bubble + BM group was 48% greater than the control ( $P < 0.01$ ). US + Bubble stimulation induces the expression of adhesion molecules (VCAM-1 and ICAM-1) in capillaries, and the US + Bubble-mediated supply of BM-MNCs increased the myocardial content of VEGF and bFGF. The left ventricular wt/body wt, area of cardiac fibrosis, and apoptotic cell numbers in the US + Bubble + BM group significantly ( $P < 0.05$ ) decreased by 82%, 73%, and 64% relative to the control, respectively. The cardiac function in myopathic hamsters (assessed by fractional shortening) was markedly improved 36% ( $P < 0.05$ ) by US + Bubble + BM treatment. Targeted delivery of BM-MNCs by US + Bubble to the myocardium of the cardiomyopathic hamster increased the capillary densities and regional blood flow and inhibited cardiac remodeling, resulting in the prevention of heart failure. This non-invasive cell delivery system may be useful as a novel efficient approach for angiogenic cell therapy to the myocardium.

© 2006 Elsevier Inc. All rights reserved.

**Keywords:** Angiogenesis; Endothelial progenitor; Ultrasound; Microbubble; Cardiomyopathy

### 1. Introduction

Cardiovascular diseases are often caused by a decrease in blood perfusion. Medical interventions to restore blood supply cannot be applied to all the patients. To treat those who are not candidates for

conventional revascularization, alternative salvage therapy for neovascularization needs urgently to be developed. Recently, bone-marrow-derived endothelial progenitor cells (BM-EPCs) were isolated from the mononuclear cell (MNC) population in the peripheral blood [1,2]. These cells have a high proliferative activity and differentiated into ECs [2], suggesting that they may have the potential to accelerate neovascularization in the ischemic tissue. EPCs that were expanded from the adult peripheral or the cord blood

\* Corresponding author. Fax: +81 75 251 5514.

E-mail address: [okigakim@koto.kpu-u.ac.jp](mailto:okigakim@koto.kpu-u.ac.jp) (M. Okigaki).

enabled the increase in the capillary density (CD) in the ischemic hindlimb [3,4]. Based on this basic research, the intramuscular transplantation of BM-MNCs has been clinically applied to induce angiogenesis in the ischemic limb [5]. Furthermore, clinical trials of catheter-based autologous BM-MNCs delivery approaches, intracoronary transfer for acute myocardial infarction [6–9], or intramyocardial injection for ischemic cardiomyopathy [10–12] resulted in an improvement of symptoms, blood perfusion, and function.

Besides obtaining diagnostic ultrasound (US) images, contrast agent microbubbles have been currently used for therapeutic purposes. US-mediated microbubble destruction in the capillary lumen elicits arteriogenesis and enhanced the hyperemic blood flow in normal [13] and ischemic [14] rat skeletal muscle. Microbubble destruction creates pores in the capillary walls, and this effect is dependent on the applied ultrasound power [13,15–17]. This method was applied to the targeted drug and gene delivery to the arterial vasculature [18,19] and tissue [20–23]. Targeted transfer of hepatocyte growth factor gene by US-microbubble destruction to cardiomyopathic hearts leads to the prevention of myocardial injury through angiogenesis actions [24,25].

Deterioration of cardiac function in the BIOTO2 cardiomyopathic hamster is attributed to a defect in  $\delta$ -sarcoglycan that disrupts the dystrophin-associated glycoprotein complex, in which myocyte loss progresses in two ways. First, numerous vessel segments with constrictions and focal luminal narrowing develop. These vessel irregularities lead to focal ischemic injury and necrosis, resulting in myocyte loss [26]. Second, myocyte loss progresses owing to  $\text{Ca}^{2+}$  overload caused by high basal activity of  $\text{Ca}^{2+}$ -permeable channels or mechanosensitive  $\text{Ca}^{2+}$ -permeable channels [27]. In fact, Shimizu et al. [28] demonstrated the decreases in capillary numbers in the BIOTO2 myocardium by the histological examination and angiography using synchrotron radiation and concluded that impaired neoangiogenesis is involved in the progression of cardiac function in the BIOTO2. Furthermore, since Taniyama et al. reported that the angiogenic gene therapy using hepatic growth factor (HGF) effectively increases the regional blood flow and prevents the progression of heart failure in the similar cardiomyopathic hamster BIO14.6 model [24]. Based on these previous findings, we attempted to study whether the increase in the regional blood perfusion by angiogenic cell therapy can prevent the progression of myocyte injury in the BIOTO2 hamster model.

The present study demonstrates that the intravenous infusion of BM-MNCs combined with US + Bubble enabled targeted delivery of BM-MNCs to the BIOTO2 myopathic hearts and induced the regional angiogenic response, resulting in an improvement of heart failure associated with the inhibition of cardiac remodeling and myocyte apoptosis. These findings suggest that this novel targeted cell delivery approach may be feasible as a non-invasive angiogenic cell therapy to the myocardium.

## 2. Materials and methods

### 2.1. Isolation of MNCs from the bone marrow

BM-MNCs were isolated by Percoll gradient centrifugation (Nycoprep, AXIS-SHIELD, Oslo, Norway) [29]. All animal

experiments were approved by the Animal Care and Use Committee of Kyoto Prefectural University.

### 2.2. BM-MNCs delivery into the myocardium with microbubble-US

Eight-week-old BIOTO2 hamsters (Bio Breeders, Fitchburg, MA) were irradiated with low-frequency US (1 MHz, 50% duty ratio; ITO-US-3, Ito Co. Ltd, Tokyo, Japan) at an intensity of  $2.0 \text{ W/cm}^2$  for 90 s, along with the intravenous injection of 200  $\mu\text{l}$  microbubble (Optison, Mallinckrodt Inc) and 300  $\mu\text{l}$  saline, including  $1 \times 10^8$  BM-MNCs. To prevent allograft rejection, recipients were administered immunosuppressant FK-506 (1 mg/kg/day; Fujisawa Pharmaceutical Co., Osaka, Japan) using a mini-osmotic pump (Alzet 2004; Alza Co, Palo Alto, CA).

### 2.3. Tracking donor BM-MNCs

Donor BM-MNCs were labeled with 1,1'-dioctadecyl-3,3',3'-tetramethylindocarbocyanine perchlorate (DiI, Molecular Probes, Inc) and infused to the recipient animals. After the indicated periods, hearts were frozen-sectioned and incubated with anti-von Willebrand factor (vWF) antibody (Santa Cruz Biotechnology, Inc, sc-8068) followed by FITC-conjugated secondary antibody. DiI+/vWF+ double-positive fluorescent cells were evaluated.

### 2.4. Histological and immunohistochemical analyses

Twelve weeks after BM-MNC delivery, the frozen-sectioned hearts were stained by alkaline phosphatase (ALP) with indoxyl tetrazolium to measure viable vessel densities in randomly selected, ten microscopic fields. The paraffin-sectioned samples were also stained with Hematoxylin-Eosin or Sirius red, and the area of cardiac muscle fiber and collagen content was evaluated, respectively. Apoptotic cardiomyocytes were evaluated in frozen-sectioned samples with an In situ Cell Death detection kit (Roche) with diaminobenzidine (DAB) and counterstained with 0.5% methyl green (Sigma). For VCAM-1, ICAM-1, interleukin 1-beta (IL-1 $\beta$ ), tumor necrosis factor-alpha (TNF- $\alpha$ ), monocyte chemoattractant protein-1 (MCP-1), and macrophage/monocyte immunostaining, we used the rat model as their anti-hamster antibodies were not available. Two days after US + Bubble treatment to the Wistar rats, the paraffin-sectioned hearts were immunostained by anti-rat VCAM-1 (Santa Cruz Biotechnology), ICAM-1 (ENDOGEN), IL-1 $\beta$  (Santa Cruz Biotechnology), TNF- $\alpha$  (Biosource), MCP-1 (Abcam), and CD68 (ED-1, Serotec) with DAB counterstained with Hematoxylin. The frozen-sectioned hearts were also immunostained with anti-FITC-conjugated rat VCAM-1 or anti-PE-conjugated rat vWF antibodies (BD Pharmingen). Double immunostaining using anti-rat VCAM-1 (horse radish peroxidase: brown) and anti-CD68 (alkaline phosphatase: red) antibodies with DAB and naphtol, respectively, was also performed.

### 2.5. Immunocytochemistry

$1 \times 10^5$  BM-MNCs were primarily cultured on fibronectin-coated chamber slides (Becton Dickinson) for 7 days with EBM-2 medium supplemented with 5%FBS, EGM-2-MV-SingleQuots (Clonetics), and then incubated with 2.4  $\mu$ l/ml of DiI-labeled acetylated LDL (Molecular Probes) and 10 ng/ml of BS-1-FITC (Sigma). The double-stained cells were counted as EPCs.

### 2.6. Western blot and real-time polymerase chain reaction (PCR) analysis

At the indicated period after BM-MNCs infusion, the hamster LV lysates were subjected to Western blot analysis with antibodies against VCAM-1 and ICAM-1 (Santa Cruz Biotechnology) or antibodies against VEGF (R&D Systems) and basic FGF (Upstate), respectively, and visualized using an ECL detection kit (Amersham).

Two days after US + Bubble treatment to the Wistar rats, total RNA was extracted from LV and then the real-time PCR was performed using the commercial kit (QIAGEN). The IL-1 $\beta$ , TNF- $\alpha$ , and MCP-1 mRNA amounts in the US + Bubble-treated heart were compared with that of the non-treated group.

### 2.7. Monitoring cardiac blood flow with $^{99m}$ Tc-Tetrofosmin scintigraphy

Cardiac blood flow was evaluated with the ratio of cardiac uptaken to the total dosed radioactivity of  $^{99m}$ Tc-Tetrofosmin. The frozen short-axis-sectioned hearts (50  $\mu$ m thickness) at the mid-ventricle level were exposed to an imaging plate, and a radioactive image was obtained using a Bio Imaging Analysis System (FUJI Photo Film).

### 2.8. Evaluation of the ventricular dimension and function by echocardiography

Transthoracic M-mode echocardiogram (SONOS 5500; Hewlett-Packard) was obtained by the parasternal short axis at mid-papillary muscle levels, and the LV end-diastolic dimension (LVdD) and percent fractional shortening (%FS) were determined.

### 2.9. Statistics

Statistical analyses were performed with one-way ANOVA followed by pair-wise contrasts using Dunnett's test. Data

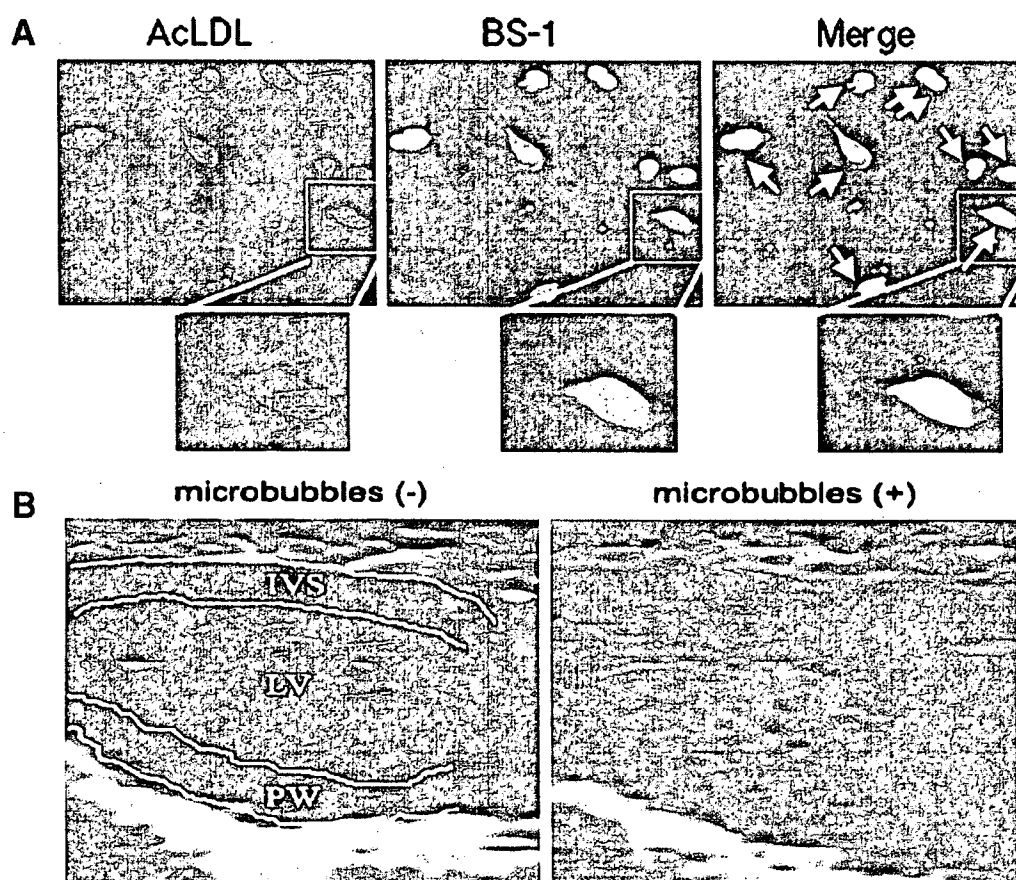


Fig. 1. EPC properties of BM-MNCs and the echocardiographic microbubble image. (A) BM-MNCs were cultured on fibronectin-coated plates for 7 days, and their binding ability to FITC-BS-1-Lectin and uptake of DiI-AcLDL was examined. BS-1+/AcLDL+ double fluorescent cells (arrows) in the merged image are considered to be the endothelial-lineage cells that exhibit a spindle shape. (B) The echocardiographical image (arrows) of microbubble delivery into the LV cavity immediately after microbubble injection. LV: left ventricle, IVS: intra-ventricular septum, PW: posterior wall. Scale bar indicates 100  $\mu$ m.

(means  $\pm$  SE) were considered statistically significant when  $P$  was  $<0.05$ .

### 3. Results

#### 3.1. Incidence of endothelial-lineage cells in BM-MNCs

Immunocytochemical analysis indicated that  $76 \pm 2\%$  of 7-day-cultured BM-MNCs (prepared from the BIOTO2 hamster) incorporated DiI-AcLDL and bound FITC-BS-1 ( $n = 5$ ), some of which exhibited a spindle shape (Fig. 1A), suggesting that endothelial-lineage cells were considered to be included in this fraction as reported [5,30].

#### 3.2. Targeted delivery of BM-MNCs to the myocardium by ultrasound-mediated microbubble destruction

US was applied to the anterior chest for 90 s immediately after intravenous injection of microbubble (Optison<sup>®</sup>) into the BIOTO2 hamster followed by infusion of DiI-labeled  $1 \times 10^8$  BM-MNCs. Echocardiography confirmed that microbubble was actually delivered into the LV cavity a few seconds after injection (Fig. 1B).

The transfused DiI-positive BM-MNCs were detected in the myocardium 2 weeks after US + Bubble stimulation but barely detectable by the US treatment alone without microbubble injection ( $121.2 \pm 24.5$  vs.  $2.8 \pm 1.3$  cells/ $\text{mm}^2$ ,  $n = 10$ ,  $P < 0.001$ ) (Fig. 2A). The DiI-positive BM-MNCs were mostly merged with endothelial marker vWF-positive microvessels (the merge panel in Fig. 2A), while no DiI+ cells were merged in the cardiomyocytes immunostained by cardiac  $\alpha$ -myosin heavy chain (data not shown). Interestingly, DiI+ BM-MNCs were found to be attaching onto the endothelium of the microvessel 2 days after US + bubble stimulation (Fig. 2B).

#### 3.3. US + Bubble + BM-MNCs treatment increased the capillary density and prevented cardiac remodeling

Capillary densities (CD) were evaluated by counting ALP+ viable capillaries. We found that the CD of the 20-week-old BIOTO2 hamster were decreased ( $48 \pm 3\%$ ,  $P < 0.005$ ) than the normal (F1B) hamsters and the US + Bubble + BM treatment significantly ( $P < 0.01$ ) increased the CD (Fig. 3A), whereas there was no significant difference in the CD/myocyte ratio between the treated and untreated BIOTO2 hamsters

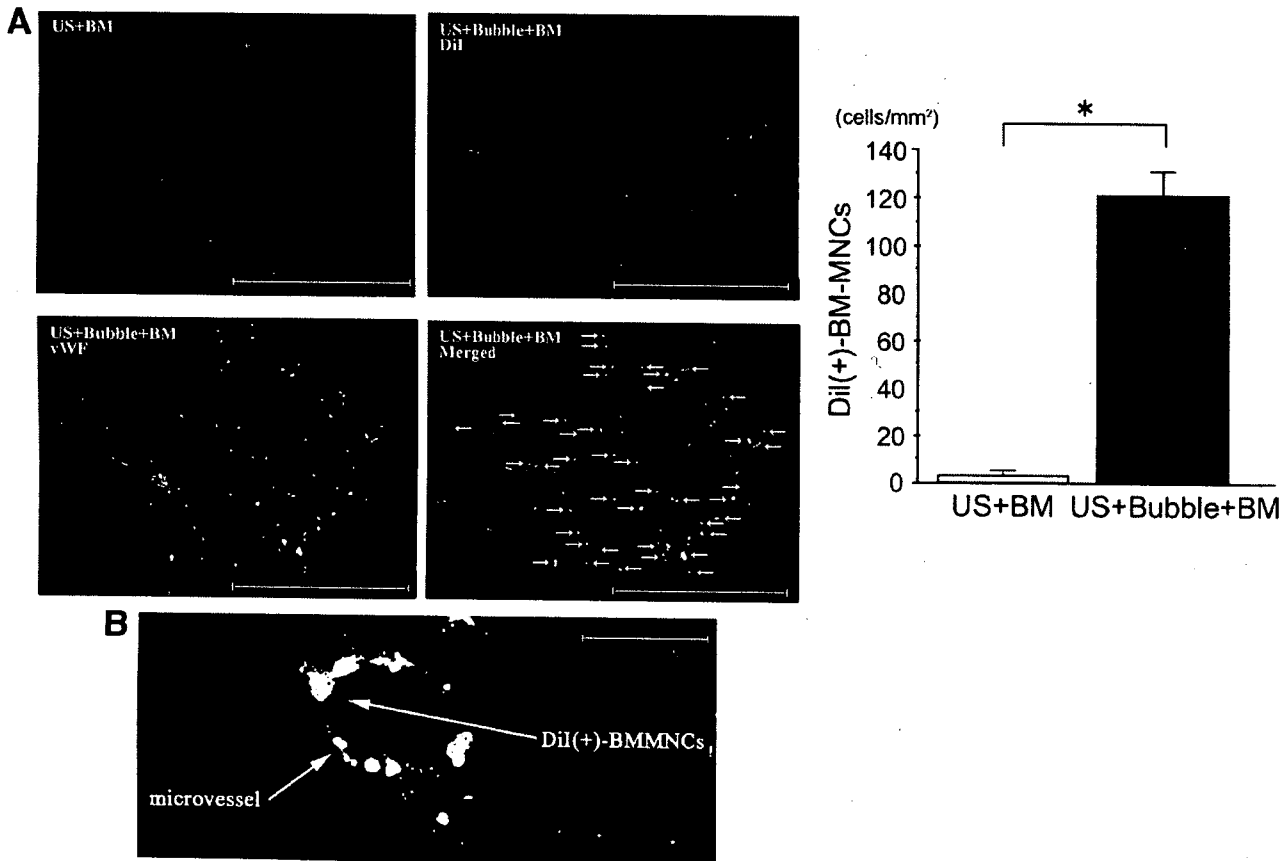


Fig. 2. Fluorescence micrograph of BM-MNCs transplanted by US + Microbubble. (A) US was applied to the anterior chest immediately after intravenous infusion of DiI-labeled BM-MNCs ( $1 \times 10^8$  cells) with microbubble (US + Bubble + BM) or without microbubble (US + BM). DiI+ BM-MNCs (red color) and vWF+ microvessels (green color) in the myocardial samples at 14 days after US + Bubble stimulation are shown. Calculated DiI+ cell numbers were significantly higher in US + Bubble + BM group than that in US + BM group ( $n = 10$ ,  $*P < 0.001$ ). DiI+ cells mostly corresponded to vWF+ microvessels in the merged image (arrows). Scale bars indicate 200  $\mu\text{m}$ . (B) Attachment of DiI+ BM-MNCs onto the endothelial layer of the microvessel 2 days after US + bubble stimulation. Scale bar indicates 20  $\mu\text{m}$ .

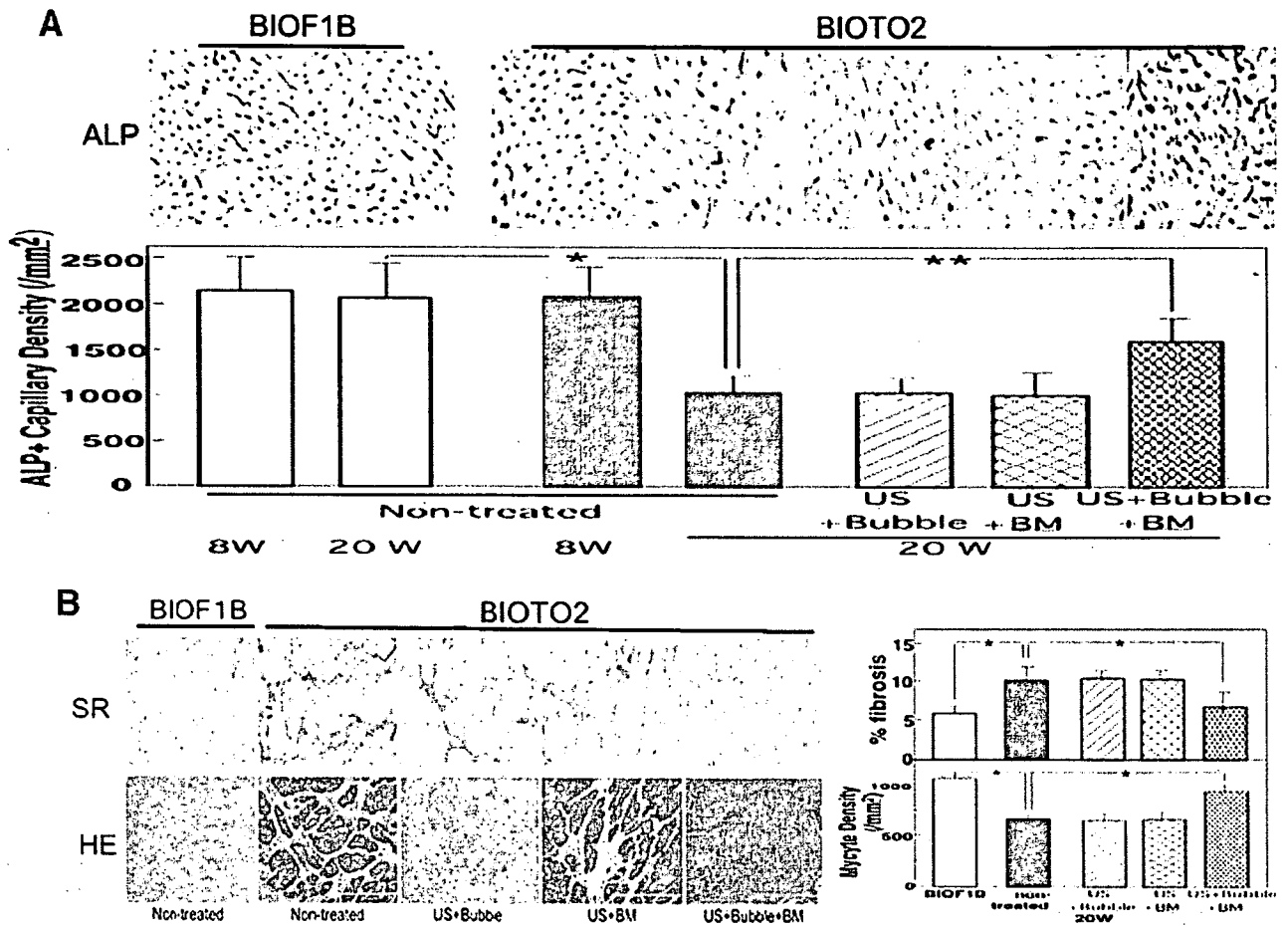


Fig. 3. Histological analysis of myopathic hearts treated with US + microbubble. (A) Evaluation of the capillary density (CD): 8-week-old hamsters were treated with US + microbubble + BM-MNCs infusion (US + Bubble + BM) ( $n = 12$ ), US + microbubble (US + Bubble) ( $n = 5$ ), and US + BM-MNC infusion (US + BM) ( $n = 5$ ) or non-treated ( $n = 10$ ). The LVs of 8- and 20-week-old BIOTO2 or control (BIOF1B) hamsters ( $n = 6$ ) were frozen-sectioned and stained for alkaline phosphatase (ALP), and the number of ALP+ capillaries (blue dots) was counted. Representative images and statistical analysis were shown. \* $P < 0.005$ , \*\* $P < 0.01$ . (B) Evaluation of the cardiac fibrosis and myocyte density: LVs were frozen-sectioned or paraffin-sectioned and stained for Sirius red (SR) or Hematoxylin–Eosin (HE), respectively. Collagen deposition is shown as red color area in SR, while the muscle fibers were stained red in HE. Statistical analysis of the percent fibrosis (fibrotic area ratio to a total microscopic field) and the myocyte density is presented. \* $P < 0.01$ . Scale bars in panels A and B indicate 200  $\mu\text{m}$ .

(US + Bubble:  $1.45 \pm 0.15$ , US + BM:  $1.52 \pm 0.09$ , US + Bubble + BM:  $1.46 \pm 0.08$ , non-treated:  $1.49 \pm 0.08$ ,  $n = 6$  each). The decrease in myocyte densities in the untreated BIOTO2 hamsters relative to the US + Bubble + BM-treated hamsters (Fig. 3B) may account for the lack of significant difference in the CD/myocyte ratio. The compensatory

hypertrophy of remaining cardiomyocytes may be also involved in this discrepancy. Similar findings (the discrepancy between CD and CD/myocyte ratio) were previously reported in the BIOTO2 hamsters [28].

The cardiac fibrosis and myocyte density were evaluated by Sirius red (SR) and Hematoxylin–Eosin (HE) staining,

Table 1  
Body weight, ventricular weight, and heart rate data at the age of 20 weeks

	BW (g)	LVW (mg)	LVW/BW (mg/g)	HR (beats/min)
Non-treated ( $n = 10$ )	$99.40 \pm 8.859$	$299.3 \pm 12.49$	$3.037 \pm 0.339$	$308.7 \pm 27.11$
US + Bubble ( $n = 5$ )	$94.80 \pm 4.147$	$294.8 \pm 16.14$	$3.111 \pm 0.158$	$318.6 \pm 24.45$
US + BM ( $n = 5$ )	$96.00 \pm 12.33$	$291.2 \pm 21.63$	$3.074 \pm 0.462$	$305.0 \pm 28.32$
BM + US + Bubble ( $n = 12$ )	$103.7 \pm 9.957$	$264.1 \pm 15.15^{***,§,j}$	$2.564 \pm 0.236^{*,§,j}$	$315.8 \pm 25.59$

Values are means  $\pm$  SD; control = BIOTO2 treated with intravenous administration of BM-MNCs-free 0.9% saline solution; US + Bubble = BIOTO2 treated with only ultrasound irradiation with microbubble contrast agents administration; BM = BIOTO2 treated with intravenous administration of BM-MNCs without ultrasound irradiation nor microbubble contrast agents administration; BM + US + Bubble = BIOTO2 treated with intravenous administration of BM-MNCs with ultrasound irradiation under microbubble contrast agents administration; BM-MNCs = bone marrow mononuclear cells; BW = body weight; LVW = left ventricular weight; HR = heart rate.

\* $P < 0.05$  vs. control; \*\* $P < 0.01$  vs. control; § $P < 0.05$  vs. US; j $P < 0.05$  vs. BM.

respectively (Fig. 3B). Extensive cardiac fibrosis and the decrease in myocyte density were observed in the untreated myopathic BIOTO2 hamster, as previously described [28]. The fibrosis and myocyte density were significantly recovered 27% and 36% by the US + Bubble + BM treatment, respectively (Fig. 3B). The number of the apoptotic cells in the US + Bubble + BM group was 23% less than the non-treated control group ( $0.53 \pm 0.12$ ,  $n = 12$  vs.  $0.69 \pm 0.01/\text{mm}^2$ ,  $n = 10$ ,  $P < 0.01$ ). LV weight of myopathic hamsters treated by the US + Bubble + BM-MNCs was decreased  $\sim 17.5\%$  ( $P < 0.01$ ) compared with those in the non-treated control, US + Bubble alone or BM injection groups (Table 1). Thus, BM-MNCs transplanted by the US + Bubble stimulation enhance neovessel formation in myopathic hearts and inhibited the cardiac remodeling, including interstitial fibrosis and cell apoptosis.

### 3.4. Increase in blood perfusion improved the cardiac function in the US + Bubble + BM-treated heart

Regional blood perfusion was evaluated by  $^{99\text{m}}\text{Tc}$ -Tetrofosmin scintigraphy (Fig. 4A). The  $^{99\text{m}}\text{Tc}$ -Tetrofosmin uptake was decreased all over the untreated myopathic heart, whereas the distribution of radioactivity was homogenously increased in the US + Bubble + BM-MNC infusion group and the total dosed radioactivity (% uptake) of  $^{99\text{m}}\text{Tc}$ -Tetrofosmin was 1.2-fold greater ( $n = 5$ ,  $P < 0.01$ ) than that in the non-treated group (Fig. 4A, right panel). Thus, US + Bubble + BM-MNC treatment was shown to actually increase the regional blood perfusion in the myopathic hamster heart.

To examine the in vivo consequence of improvement of myocardial blood perfusion by US + Bubble + BM-MNC treatment, we analyzed the cardiac function, LV diastolic

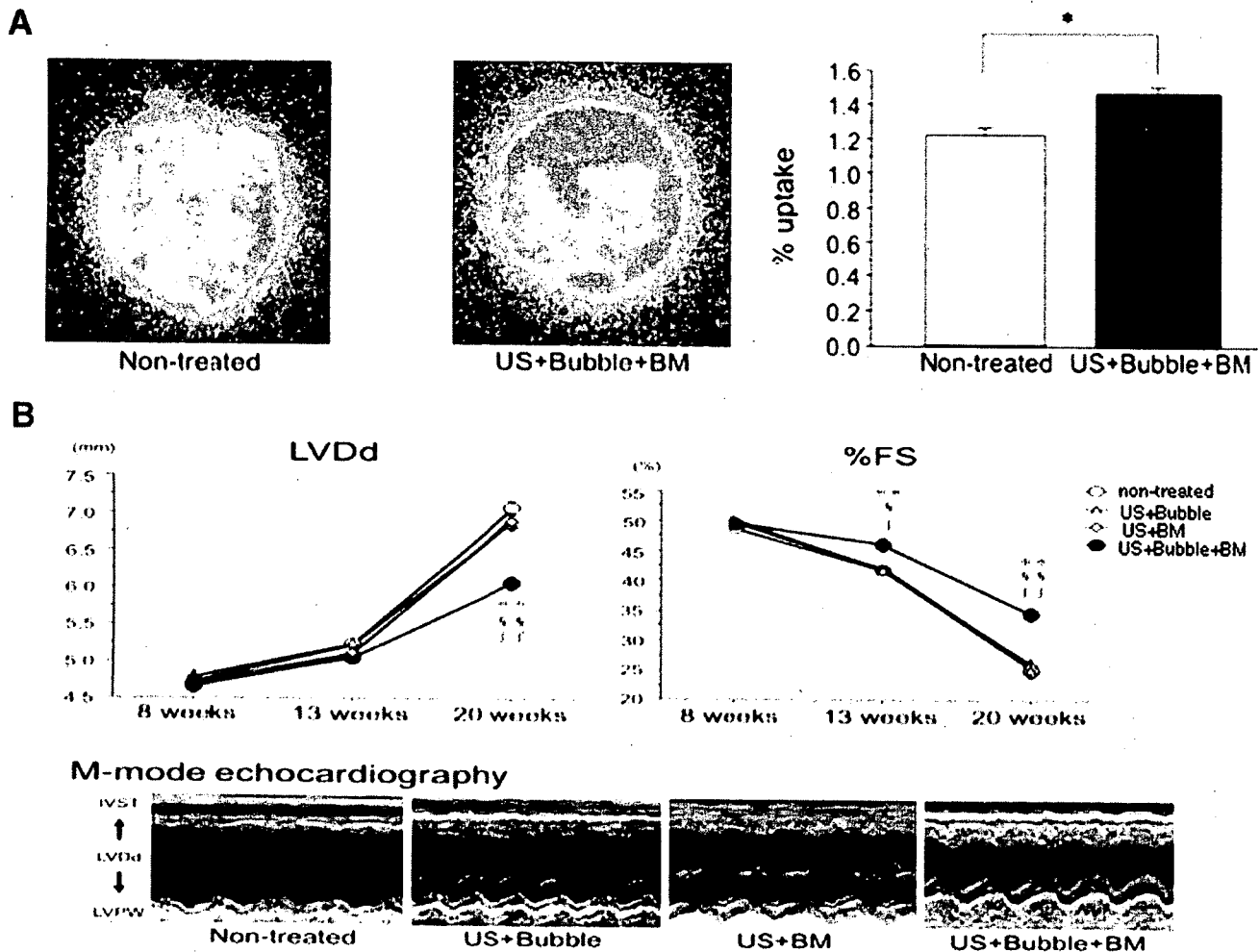


Fig. 4. Increase in blood perfusion improves the cardiac function of US + Bubble + BM-treated cardiomyopathy hamster. (A) Blood perfusion in the myocardium was evaluated by  $^{99\text{m}}\text{Tc}$ -Tetrofosmin scintigraphy 12 weeks after US + microbubble + BM-MNCs infusion (US + Bubble + BM). Yellow and orange color indicate lower and higher blood perfusion, respectively. Myocardial  $^{99\text{m}}\text{Tc}$ -Tetrofosmin uptake relative to the total dosed radioactivity (percent uptake) is evaluated in the right panel. The percent uptake was 1.2-fold higher ( $n = 5$ ,  $P < 0.01$ ) in the US + Bubble + BM-treated hamsters than in the non-treated group. \* $P < 0.01$  vs. non-treated control. (B) Evaluation of LV function by echocardiography. BIOTO2 hamsters (8-week-old) were treated with US + Bubble, US + BM, and US + Bubble + BM. LV functions were evaluated on Weeks 8, 13, and 20. Representative images on Week 20 are shown in the lower panel. The LV diastolic diameter (LVDd), fractional shortening (%FS), intra-ventricular septum (IVST), left ventricular posterior wall (LVPW), \*\* $P < 0.01$  vs. non-treated, § $P < 0.05$  vs. US + Bubble, §§ $P < 0.01$  vs. US + Bubble, † $P < 0.05$  vs. US + BM, †† $P < 0.01$  vs. US + BM.

diameter (LVDD), and fractional shortening (%FS) by echocardiography on Weeks 8, 13, and 20 after treatment in the non-treated control, US + Bubble-, US + BM-MNCs-, and US + Bubble + BM-MNCs-treated groups (Fig. 4B). All parameters of Week 8 were not significantly different between each group. On Week 13, there were no significant differences in LVDD among each group, while %FS in the US + Bubble + BM-MNCs group was appreciably improved ( $11.1 \pm 0.1\%$ ,  $P < 0.05$ ) compared with the non-treated control, and the effect was more apparent at Week 20 ( $40.2 \pm 0.2\%$ ,  $P < 0.01$ ). At Week 20, the LVDD in the US + Bubble + BM-MNC group was also significantly improved over the control ( $18.4 \pm 0.2\%$ ,  $P < 0.01$ ). There were no changes in the LVDD and %FS between the non-treated control, US + Bubble, and US + BM-MNC treatment groups. Consistent with these parameters, the motion dynamics of the posterior wall and septum were apparently improved in US + Bubble + BM-MNC group (Fig. 4B, lower panel).

### 3.5. Expression of angiogenic growth factors by the transplanted BM-MNCs

We previously reported that BM-MNCs produce VEGF and bFGF that play a major role in the induction of neocapillary formation after BM-MNCs implantation into ischemic limbs [5,30] and myocardium [31]. We therefore examined the expression of VEGF and bFGF in the myopathic hearts in which BM-MNCs were transplanted by US + Bubble. Western

blot analysis revealed that US + Bubble + BM-MNCs treatment markedly increased the expression of VEGF and bFGF ( $P < 0.001$ , 2.6-fold and 2.3-fold, respectively) compared with the non-treated control, while neither US + BM-MNCs nor the US + Bubble-treated groups showed significant changes (Fig. 5).

### 3.6. Induction of adhesion molecules and inflammatory cytokines by US + Bubble treatment

We next examined the possibility that US + Bubble treatment stimulates the expression of the adhesion molecules, causing the adhesion of transfused BM-MNCs or monocyte/macrophage onto the endothelial layer, as observed in Fig. 2B. Western blotting showed that the expressions of the adhesion molecules VCAM-1 and ICAM-1 increased to  $\sim 2.5$ -fold ( $P < 0.01$ ) in the US + Bubble- or US + Bubbles + BM-MNCs-treated myocardium compared with the non-treated control, whereas only Bubble- or only US-treated groups did not induce the significant expression (Fig. 6A). To study the tissue localization of the adhesion molecules and monocyte/macrophages (CD68), we performed the immunohistochemical analysis. As the anti-hamster antibodies positive for VCAM-1, ICAM-1, and CD68 were not available, we prepared the rat myocardial samples 3 days after US + Bubble treatment and used the anti-rat antibodies for immunostaining. We found that the expressions of VCAM-1 and ICAM-1 were localized in the vWF+ vessels in the US + Bubble-treated myocardium (Fig. 6B, ICAM-1 not shown), whereas no expression was observed in the untreated

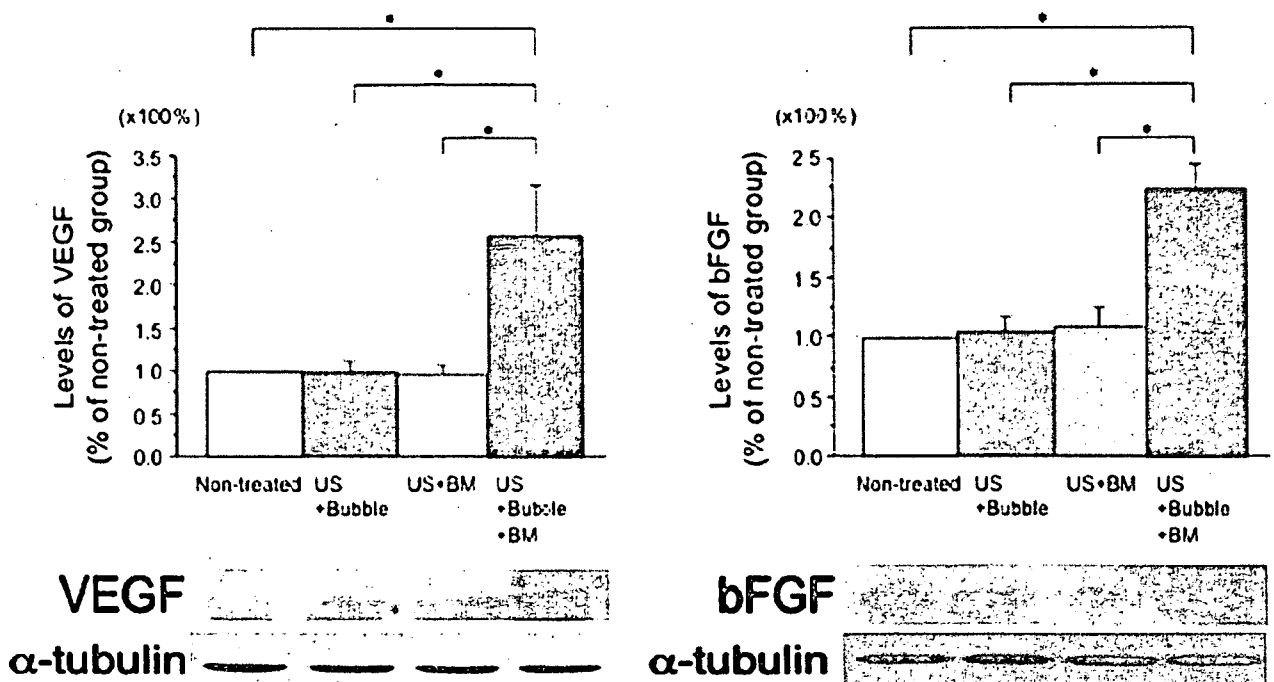


Fig. 5. Expression of angiogenic growth factors. Three days after US + BM, US + Bubble, or US + Bubble + BM treatment ( $n = 5$ , each), LV lysates were immunoblotted with the anti-VEGF, anti-basic FGF (bFGF), and anti- $\alpha$ -tubulin antibodies. The signal densities of VEGF and bFGF were arbitrarily normalized by that of  $\alpha$ -tubulin. \* $P < 0.001$ .



control (Fig. 6C). The CD68<sup>+</sup> macrophages were markedly infiltrated in the US + Bubble-treated myocardium (Fig. 6C, left panel), in which CD68<sup>+</sup> cells mainly adhered onto the inner lumen of VCAM-1<sup>+</sup> vessels and were partly observed in the interstitial region around the vessels (Fig. 6C, right panel), suggesting that the induction of the adhesion molecules in the US + Bubble-treated vessels caused the infiltration of macrophages into the interstitial region of myocardium.

We also examined the expression of TNF- $\alpha$ , IL-1 $\beta$ , and MCP-1 by the real-time PCR and immunohistochemical analysis. As the anti-hamster antibodies positive for MCP-1, TNF- $\alpha$ , and IL-1 $\beta$  were not available, we prepared the rat myocardial samples 3 days after US + Bubble treatment and used the anti-rat antibodies for immunostaining. The real-time PCR showed that their expressions are markedly elevated (approximately 7- to 15-fold,  $P < 0.001$ ) compared with those in

the non-treated control (Fig. 7A). The immunohistochemical analysis revealed that these cytokines (MCP-1, TNF- $\alpha$ , and IL-1 $\beta$ ) were mainly expressed in the vessels in the US + Bubble-treated myocardium (Fig. 7B).

#### 4. Discussion

A new delivery system of drugs or genes has been developed using US-targeted microbubble destruction. The drugs or genes that attach onto gas-filled microbubbles circulate through the intravascular space and are mechanically destroyed within the target organ by US [18,19,21,32], whereas no studies have been reported that determine whether this method is feasible for delivering the “vascular progenitor cells” to specific vascular sites. US-targeted microbubble destruction was reported to have an inflammatory action on

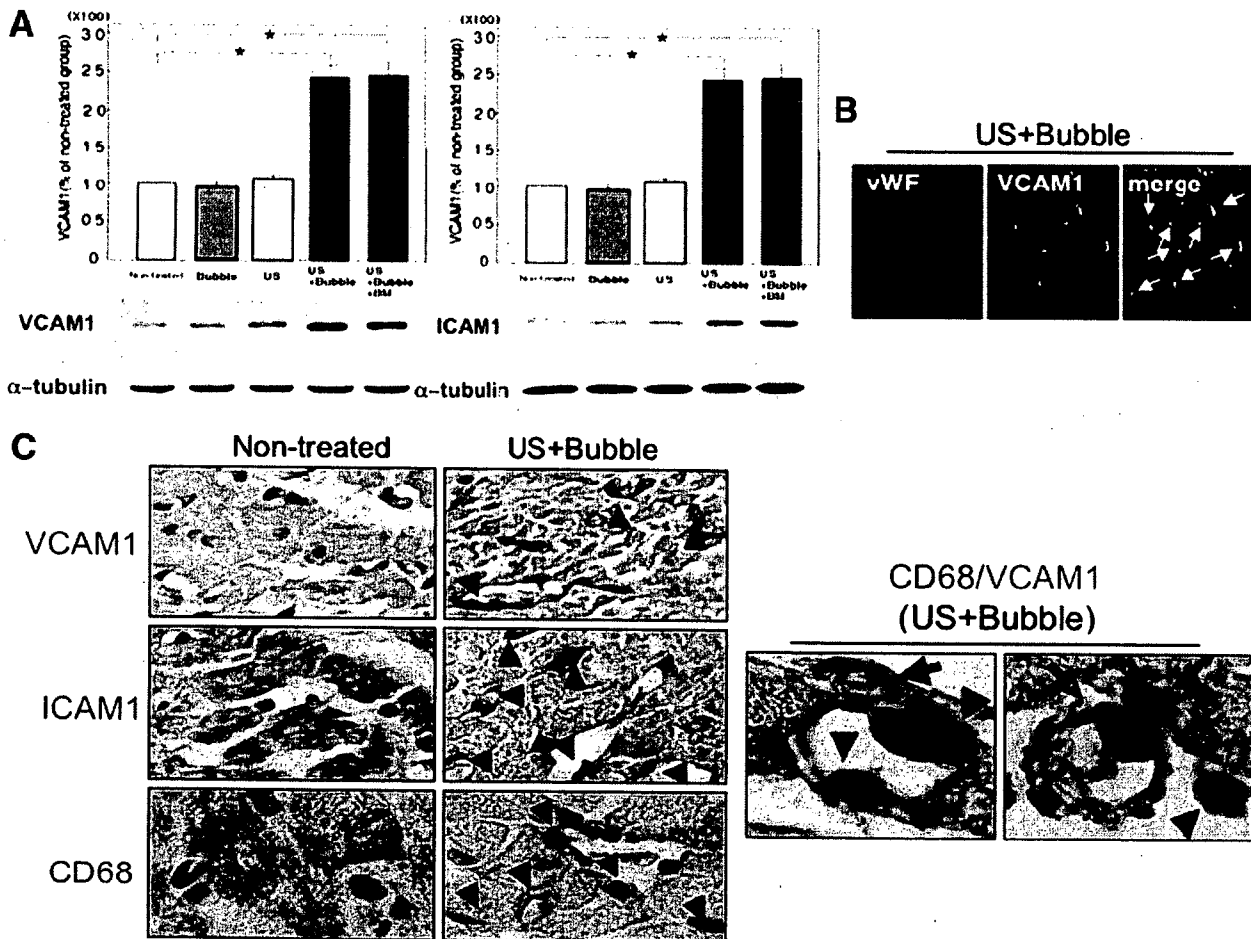


Fig. 6. Expression of adhesion molecules in US + Bubble-treated heart. (A) Two days after Bubble alone, US alone, US + Bubble, or US + Bubble + BM treatment, LV lysates were subjected to the immunoblot analysis using anti-VCAM-1, anti-ICAM-1, and anti- $\alpha$ -tubulin antibodies. Signal densities of VCAM-1 and ICAM-1 were arbitrarily normalized by  $\alpha$ -tubulin. The expression of VCAM-1 and ICAM-1 was significantly ( $*P < 0.01$ ) increased to 2.3- and 2.2-fold to compared the non-treated control, respectively. (B) For immunohistochemistry, we used the rat model as the hamster antibodies were not available. Frozen-sectioned rat LV samples (3 days after US + Bubble treatment) were immunostained with anti-rat vWF and anti-rat VCAM-1 antibodies followed by Rhodamin- or FITC-labeled secondary antibodies. VCAM-1 positive cells mostly corresponded to vWF positive vessels. Scale bar indicates 200  $\mu$ m. (C) Two days after US + Bubble treatment, paraffin-sectioned rat LVs were immunostained using the antibodies against rat VCAM-1, ICAM-1, or CD68 (macrophage-specific antigen) with DAB or naphthol, respectively. Arrowheads in panel C, left panels indicate the VCAM-1<sup>+</sup> or ICAM-1<sup>+</sup> capillaries and CD68<sup>+</sup> cells. Double fluorescence images using anti-rat CD68<sup>+</sup> and anti-rat VCAM-1<sup>+</sup> antibodies are presented in the right panels. CD68<sup>+</sup> cells (red arrowheads) mainly adhered onto the inner lumen of VCAM-1<sup>+</sup> vessels (brown arrows) or were partly observed in the interstitial region around the vessels.

the cell surface by making small holes that revert to a normal appearance within 24 h [13]. Song et al. [14,23] reported that US-targeted microbubble destruction causes capillary rupturing that stimulates neovessel formation and an increase in blood flow in both normal and ischemic skeletal muscles. We previously demonstrated that the recruitment of BM-MNCs stimulates angiogenesis in ischemic muscles by releasing angiogenic factors, including VEGF or bFGF and by the supply of endothelial progenitors [29,30]. Furthermore, we reported that BM-MNCs had a higher adhesive activity on the endothelium than did peripheral blood MNCs, and this adhesive activity was dependent on the expression level of adhesion molecules on the endothelium [29]. We therefore expanded the previous studies by Song et al. [14,23] and further studied whether US-mediated microbubble destruction, combined with the intravenous transfusion of BM-MNCs, enhanced neovessel formation by an increase in the endothelial attachment of BM-MNCs, leading to improvement in blood perfusion and cardiac function of BIOTO2 cardiomyopathy caused by limited neocapillary formation [26–28]. The present study demonstrates for the first time that this novel cell delivery system enables the vascular-endothelium-targeted attachment of infused BM-MNCs and increases the neovessel formation and blood flow in myopathic hearts, resulting in an improvement of cardiac function via the inhibition of myocyte apoptosis and interstitial fibrosis. This functional recovery was not found by BM-MNCs transfusion without US + Bubble, suggesting that US + Bubble-mediated BM-MNCs delivery is highly potent for neovascularization.

US + Bubble stimulation was reported to mechanically induce pores in the capillary wall [16]. The present study showed that the expression of adhesion molecules was markedly induced by the US + Bubble-mediated response (Fig. 5) and transfused BM-MNCs actually attached onto the injured endothelial layer (Fig. 2A). The adhesion activity of BM-MNCs on the endothelial layer was reported to be markedly higher than that of the circulating MNCs, and its adhesive activity was enhanced on the balloon-injured endothelium [29]. Indeed, as we observed in Fig. 2A, BM-MNCs infusion with US + Bubble stimulation achieved much more efficient regional cell delivery than simple BMC injection. Transplantation of autologous BM-MNCs has been clinically applied for patients with ischemic heart diseases via catheter-based approaches, direct injection into the ischemic myocardium [11,12,33], or intracoronary infusion [6–9]. Although they showed favorable effects on cardiac remodeling and function, the efficiency of cell delivery was still limited and such therapies were invasive. Most of the injected BM-derived mesenchymal stem cells died 4 days after intramyocardial injection [34], and ~60% of the BM-MNCs infused by intracoronary injection were trapped by the spleen and liver, and a minor population of cells (~10%) were present in the heart [35]. We only found a transient appearance of ventricular premature beats during the 90 s of US + Bubble application, and thereafter no incidences of death were observed during the observation period in any of the treated myopathic hamsters ( $n = 48$ ). Thus, the present study suggests that US + Bubble + BM-MNC treatment is a

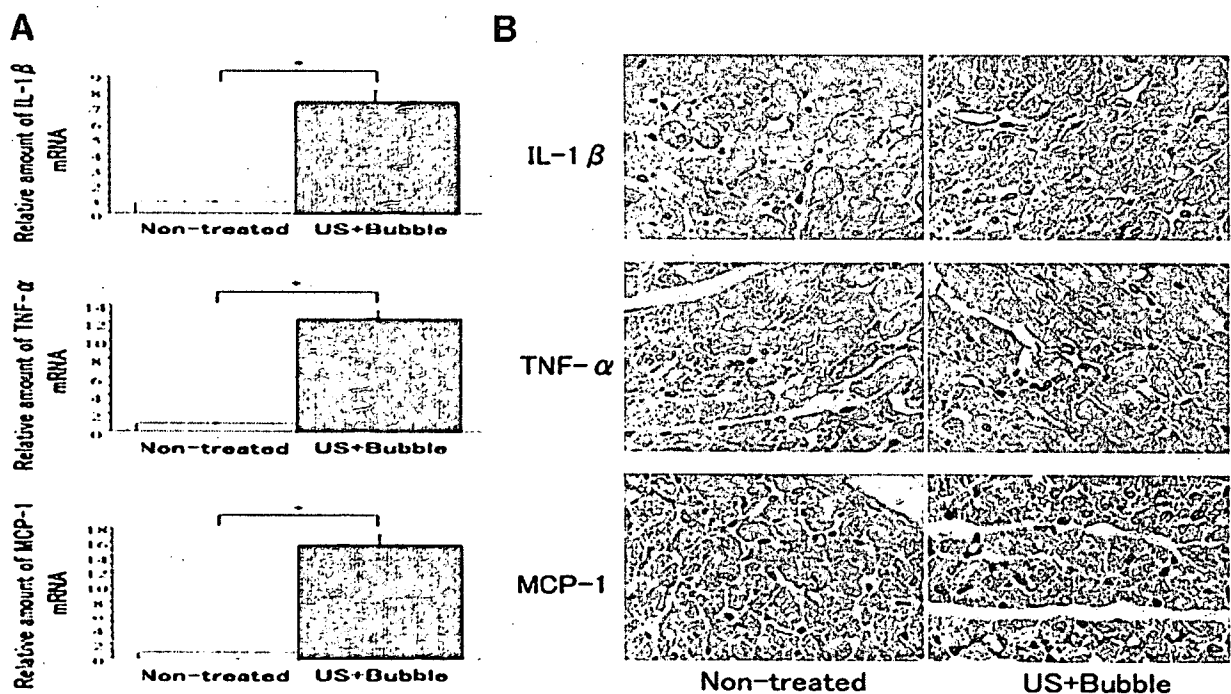


Fig. 7. US + Bubble induced the expression of inflammatory chemokine and cytokines. (A) Three days after US + Bubble treatment, total RNAs of rat LVs were subjected to the real-time PCR analysis for expression of IL-1 $\beta$ , TNF- $\alpha$ , and MCP1. Their mRNA levels in the US + Bubble-treated myocardium were significantly ( $*P < 0.001$ ,  $n = 5$  each) higher than those in the non-treated groups. (B) Rat LVs were also paraffin-sectioned and immunostained using the antibodies against rat IL-1 $\beta$ , rat TNF- $\alpha$ , and rat MCP-1. Brown dot indicates the positive cells.

safe and feasible non-invasive system for targeted cell delivery to the myocardium.

We found the adhesion of transfused BM-MNCs and the increased expressions of adhesion molecules on the US + Bubble-stimulated endothelium (Fig. 5). Considering our recent study reporting that systemically transplanted BM-MNCs can be firmly attached onto the injured vascular endothelium in an adhesive molecule-dependent manner [29], it is likely that the mechanical impact of US-mediated microbubble destruction induces the up-regulation of these adhesion molecules on the targeted vascular endothelium, causing the attachment of transfused BM-MNCs onto targeted endothelial layer. The present study clearly shows that endothelial progenitors included in BM-MNCs trans-differentiate to endothelial-like cells (Fig. 2) to repair US + Bubble-stimulated endothelium as well as supply the angiogenic factors (VEGF and bFGF) (Fig. 4) for neovessel formation. BM-MNC-derived endothelial progenitors that attached on the endothelial layer or leaked out from the injured endothelium may be incorporated into the regenerated endothelium and/or stimulate neovessel formation by supplying angiogenic factors. Thus, these synergistic bioeffects after US + Bubble + BM-MNC stimulation likely induced a potent angiogenic response in the US + microbubble-applied myocardium.

Although there is a concern that the US application to the anterior chest may cause the geometrical unevenness of the biological effects in the LV wall, there was no obvious difference in the biological effect between the anterior and the inferior LV wall in the US + Bubble + BM-treated heart, such as the CD ( $1354 \pm 222.4$  and  $1288 \pm 207.2/\text{mm}^2$ ,  $n = 5$ ) or the cardiac muscle fiber density ( $926.3 \pm 88.7$  and  $901.3 \pm 66.8/\text{mm}^2$ ,  $n = 5$ ). The diameter of the US probe (approximately 3 cm) is much bigger than the size of the hamster's heart (less than 1 cm), and furthermore the US was applied from various directions with continuously changing the angle to the chest wall, leading to achievement of the geometrically even biological effect all over the field of the myocardium.

The BIOTO2 Syrian hamsters used in this study inherit cardiomyopathy in an autosomal recessive manner and manifested dilated cardiomyopathy [36,37]. They have a genetic mutation of sarcoglycans, a subcomplex of the dystrophin-associated glycoprotein complex (DAGC) [38–40]. The impairment of the cardiac function in this hamster was caused by altered microvasculature, leading to a decrease in cardiac blood flow [26,28]. The BIOTO2 hamster exhibited a significantly lower capillary density [28] that correlated with the myocyte density and cardiac function. Angiogenetic gene therapy using hepatic growth factor was shown to enhance the angiogenic response and improve blood perfusion in the other myopathic hamster BIO14.6 model [24]. Combined with our present result using angiogenic cell therapy, it is likely that the enhancement of neovessel formation followed by an increase in regional blood flow inhibits cardiac remodeling in myopathic hearts and improves heart failure. Conclusively, BM-MNCs transplantation by US–microbubble-mediated cell delivery is a novel approach for an efficient angiogenic cell

therapy, which is the most relevant strategy for the treatment of idiopathic myopathic hearts that requires an extensive cell delivery to the myocardium.

### Acknowledgments

This study was supported in part by research grants from the Ministry of Education, Science, Sports and Culture, and the Ministry of Health, Labor and Welfare, Japan, the Study Group of Molecular Cardiology, the Japan Medical Association, and the Japan Heart Foundation.

### References

- [1] Asahara T, Murohara T, Sullivan A, Silver M, van der Zee R, Li T, et al. Isolation of putative progenitor endothelial cells for angiogenesis. *Science* 1997;275:964–7.
- [2] Asahara T, Masuda H, Takahashi T, Kalka C, Pastore C, Silver M, et al. Bone marrow origin of endothelial progenitor cells responsible for postnatal vasculogenesis in physiological and pathological neovascularization. *Circ Res* 1999;85:221–8.
- [3] Kalka C, Masuda H, Takahashi T, Kalka-Moll WM, Silver M, Kearney M, et al. Transplantation of ex vivo expanded endothelial progenitor cells for therapeutic neovascularization. *Proc Natl Acad Sci U S A* 2000; 97:3422–7.
- [4] Murohara T, Ikeda H, Duan J, Shintani S, Sasaki K, Eguchi H, et al. Transplanted cord blood-derived endothelial precursor cells augment postnatal neovascularization. *J Clin Invest* 2000;105:1527–36.
- [5] Tatchibana Yuyama E, Matsubara H, Murohara T, Ikeda U, Shintani S, Masaki H, et al. Therapeutic Angiogenesis using Cell Transplantation (TACT) Study Investigators. Therapeutic angiogenesis for patients with limb ischaemia by autologous transplantation of bone-marrow cells: a pilot study and a randomised controlled trial. *Lancet* 2002;360:427–35.
- [6] Assmus B, Schachinger V, Teupe C, Britten M, Lehmann R, Döbert N, et al. Transplantation of progenitor cells and regeneration enhancement in acute myocardial infarction (TOPCARE-AMI). *Circulation* 2002;106: 3009–17.
- [7] Britten MB, Abolmaali ND, Assmus B, Lehmann R, Honold J, Schmitt J, et al. Infarct remodeling after intracoronary progenitor cell treatment in patients with acute myocardial infarction (TOPCARE-AMI): mechanistic insights from serial contrast-enhanced magnetic resonance imaging. *Circulation* 2003;108:2212–8.
- [8] Schachinger V, Assmus B, Britten MB, Honold J, Lehmann R, Teupe C, et al. Transplantation of progenitor cells and regeneration enhancement in acute myocardial infarction: final one-year results of the TOPCARE-AMI trial. *J Am Coll Cardiol* 2004;44:1690–9.
- [9] Wollert KC, Meyer GP, Lotz J, Ringes-Lichtenberg S, Lippolt P, Breidenbach C, et al. Intracoronary autologous bone-marrow cell transfer after myocardial infarction: the BOOST randomised controlled clinical trial. *Lancet* 2004;364:141–8.
- [10] Fuchs S, Satler LF, Kornowski R, Okubagzi P, Weisz G, Baffour R, et al. Catheter-based autologous bone marrow myocardial injection in no-option patients with advanced coronary artery disease: a feasibility study. *J Am Coll Cardiol* 2003;41:1721–4.
- [11] Tse HF, Kwong YL, Chan JK, Lo G, Ho CL, Lau CP. Angiogenesis in ischaemic myocardium by intramyocardial autologous bone marrow mononuclear cell implantation. *Lancet* 2003;361:47–9.
- [12] Perin EC, Dohmann HF, Borojevic R, Silva SA, Sousa AL, Mesquita CT, et al. Transendocardial, autologous bone marrow cell transplantation for severe, chronic ischemic heart failure. *Circulation* 2003;107:2294–302.
- [13] Skyba DM, Price RJ, Linka AZ, Skalak TC, Kaul S. Direct in vivo visualization of intravascular destruction of microbubbles by ultrasound and its local effects on tissue. *Circulation* 1998;98:290–3.
- [14] Song J, Cottler PS, Klivanov AL, Kaul S, Price RJ. Microvascular remodeling and accelerated hyperemia blood flow restoration in arterially

- occluded skeletal muscle exposed to ultrasonic microbubble destruction. *Am J Physiol, Heart Circ Physiol* 2004;287:H2754–61.
- [15] Price RJ, Skyba DM, Kaul S, Skalak TC. Delivery of colloidal particles and red blood cells to tissue through microvessel ruptures created by targeted microbubble destruction with ultrasound. *Circulation* 1998; 98:1264–7.
- [16] Song J, Chappell JC, Qi M, VanGieson EJ, Kaul S, Price RJ. Influence of injection site, microvascular pressure, and ultrasound variables on microbubble-mediated delivery of microspheres to muscle. *J Am Coll Cardiol* 2002;39:726–31.
- [17] Ay T, Havaux X, Van Camp G, Campanelli B, Gisellu G, Pasquet A, et al. Destruction of microbubbles by ultrasound: effects on myocardial function, coronary perfusion pressure, and microvascular integrity. *Circulation* 2001;104:461–6.
- [18] Taniyama Y, Tachibana K, Hiraoka K, Namba T, Yamasaki K, Hashiya N, et al. Local delivery of plasmid DNA into rat carotid artery using ultrasound. *Circulation* 2002;105:1233–9.
- [19] Teupe C, Richter S, Fisslthaler B, Randriamboavonjy V, Ihling C, Fleming I, et al. Vascular gene transfer of phosphomimetic endothelial nitric oxide synthase (S1177D) using ultrasound-enhanced destruction of plasmid-loaded microbubbles improves vasoreactivity. *Circulation* 2002;105:1104–9.
- [20] Mukherjee D, Wong J, Griffin B, Ellis SG, Porter T, Sen S, et al. Ten-fold augmentation of endothelial uptake of vascular endothelial growth factor with ultrasound after systemic administration. *J Am Coll Cardiol* 2000; 35:1678–86.
- [21] Price RJ, Kaul S. Contrast ultrasound targeted drug and gene delivery: an update on a new therapeutic modality. *J Cardiovas Pharmacol Ther* 2002;7:171–80.
- [22] Shohet RV, Chen S, Zhou YT, Wang Z, Meidell RS, Unger RH, et al. Echocardiographic destruction of albumin microbubbles directs gene delivery to the myocardium. *Circulation* 2000;101:2554–6.
- [23] Song J, Qi M, Kaul S, Price RJ. Stimulation of arteriogenesis in skeletal muscle by microbubble destruction with ultrasound. *Circulation* 2002; 106:1550–5.
- [24] Taniyama Y, Morishita R, Aoki M, Hiraoka K, Yamasaki K, Hashiya N, et al. Angiogenesis and antifibrotic action by hepatocyte growth factor in cardiomyopathy. *Hypertension* 2002;40:47–53.
- [25] Kondo I, Ohmori K, Oshita A, Takeuchi H, Fuke S, Shinomiya K, et al. Treatment of acute myocardial infarction by hepatocyte growth factor gene transfer: the first demonstration of myocardial transfer of a “functional” gene using ultrasonic microbubble destruction. *J Am Coll Cardiol* 2004;44:644–53.
- [26] Factor SM, Minase T, Cho S, Dominitz R, Sonnenblick EH. Microvascular spasm in the cardiomyopathic Syrian hamster: a preventable cause of focal myocardial necrosis. *Circulation* 1982;66:342–54.
- [27] Iwata Y, Katanosaka Y, Arai Y, Komamura K, Miyatake K, Shigekawa M. A novel mechanism of myocyte degeneration involving the Ca<sup>2+</sup>-permeable growth factor-regulated channel. *J Cell Biol* 2003;161:957–67.
- [28] Shimizu T, Okamoto H, Watanabe M, Kumamoto H, Chiba S, Matsui Y, et al. Altered microvasculature is involved in remodeling processes in cardiomyopathic hamsters. *Jpn Heart J* 2003;44:111–26.
- [29] Fujiyama S, Amano K, Uehira K, Yoshida M, Nishiwaki Y, Nozawa Y, et al. Bone marrow monocyte lineage cells adhere on injured endothelium in a monocyte chemoattractant protein-1-dependent manner and accelerate reendothelialization as endothelial progenitor cells. *Circ Res* 2003;93:980–9.
- [30] Iba O, Matsubara H, Nozawa Y, Fujiyama S, Amano K, Mori Y, et al. Angiogenesis by implantation of peripheral blood mononuclear cells and platelets into ischemic limbs. *Circulation* 2002;106:2019–25.
- [31] Kamihata H, Matsubara H, Nishiue T, Fujiyama S, Tsutsumi Y, Ozono R, et al. Implantation of bone marrow mononuclear cells into ischemic myocardium enhances collateral perfusion and regional function via side supply of angioblasts, angiogenic ligands, and cytokines. *Circulation* 2001;104:1046–52.
- [32] Bekeredjian R, Chen S, Frenkel PA, Grayburn PA, Shohet RV. Ultrasound-targeted microbubble destruction can repeatedly direct highly specific plasmid expression to the heart. *Circulation* 2003;108:1022–6.
- [33] Perin EC, Dohmann HF, Borojevic R, Silva SA, Sousa AL, Silva GV, et al. Improved exercise capacity and ischemia 6 and 12 months after transcatheter injection of autologous bone marrow mononuclear cells for ischemic cardiomyopathy. *Circulation* 2004;110(11 Suppl 1):II213–8.
- [34] Toma C, Pittenger MF, Cahill KS, Byrne BJ, Kessler PD. Human mesenchymal stem cells differentiate to a cardiomyocyte phenotype in the adult murine heart. *Circulation* 2002;105:93–8.
- [35] Siminiak T, Czepczynski R, Grygieska B, et al. Evidence for extravasation of intracoronary administered bone-marrow derived CD34+ stem cells in patients with acute myocardial infarction. *Circulation* 2004;110:III-51.
- [36] Homburger F, Baker JR, Nixon CW, Wilgram G. New hereditary disease of Syrian hamsters. Primary, generalized polymyopathy and cardiac necrosis. *Arch Intern Med* 1962;110:660–2.
- [37] Jasmin G, Eu HY. Cardiomyopathy of hamster dystrophy. *Ann NY Acad Sci* 1979;317:46–58.
- [38] Roberds SL, Ervasti JM, Anderson RD, Ohlendieck K, Kahl SD, Zoloto D, et al. Disruption of the dystrophin-glycoprotein complex in the cardiomyopathic hamster. *J Biol Chem* 1993;268:11496–9.
- [39] Sakamoto A, Ono K, Abe M, Jasmin G, Eki T, Murakami Y, et al. Both hypertrophic and dilated cardiomyopathies are caused by mutation of the same gene, -sarcoglycan, in hamster: an animal model of disrupted dystrophin-associated glycoprotein complex. *Proc Natl Acad Sci U S A* 1997;94:13873–8.
- [40] Panchal BC, Trippodo NC. Systemic and regional haemodynamics in conscious Bio TO-2 cardiomyopathic hamsters. *Cardiovasc Res* 1993;27:2264–9.

# Circulation Research

JOURNAL OF THE AMERICAN HEART ASSOCIATION

American Heart  
Association® 

*Learn and Live*™

## **Erythropoietin-Mobilized Endothelial Progenitors Enhance Reendothelialization via Akt-Endothelial Nitric Oxide Synthase Activation and Prevent Neointimal Hyperplasia**

Norifumi Urao, Mitsuhiko Okigaki, Hiroyuki Yamada, Yasushi Aadachi, Kuniharu Matsuno, Akihiro Matsui, Shinsaku Matsunaga, Kento Tateishi, Tetsuya Nomura, Tomosaburo Takahashi, Tetsuya Tatsumi and Hiroaki Matsubara

*Circ. Res.* 2006;98;1405-1413; originally published online Apr 27, 2006;

DOI: 10.1161/01.RES.0000224117.59417.f3

Circulation Research is published by the American Heart Association, 7272 Greenville Avenue, Dallas, TX 75214

Copyright © 2006 American Heart Association. All rights reserved. Print ISSN: 0009-7330. Online ISSN: 1524-4571

The online version of this article, along with updated information and services, is located on the World Wide Web at:

<http://circres.ahajournals.org/cgi/content/full/98/11/1405>

Subscriptions: Information about subscribing to Circulation Research is online at <http://circres.ahajournals.org/subscriptions/>

Permissions: Permissions & Rights Desk, Lippincott Williams & Wilkins, 351 West Camden Street, Baltimore, MD 21202-2436. Phone 410-5280-4050. Fax: 410-528-8550. Email: [journalpermissions@lww.com](mailto:journalpermissions@lww.com)

Reprints: Information about reprints can be found online at <http://www.lww.com/static/html/reprints.html>

## Erythropoietin-Mobilized Endothelial Progenitors Enhance Reendothelialization via Akt-Endothelial Nitric Oxide Synthase Activation and Prevent Neointimal Hyperplasia

Norifumi Urao, Mitsuhiko Okigaki, Hiroyuki Yamada, Yasushi Aadachi, Kuniharu Matsuno, Akihiro Matsui, Shinsaku Matsunaga, Kento Tateishi, Tetsuya Nomura, Tomosaburo Takahashi, Tetsuya Tatsumi, Hiroaki Matsubara

**Abstract**—We investigated whether the mobilization of endothelial progenitor cells (EPCs) by exogenous erythropoietin (Epo) promotes the repair of injured endothelium. Recombinant human Epo was injected (1000 IU/kg for the initial 3 days) after wire injury of the femoral artery of mice. Neointimal formation was inhibited by Epo to 48% of the control ( $P < 0.05$ ) in an NO-dependent manner. Epo induced a 1.4-fold increase in reendothelialized area of day 14 denuded vessels, 55% of which was derived from bone marrow (BM) cells. Epo increased the circulating Sca-1<sup>+</sup>/Flk-1<sup>+</sup> EPCs (2.0-fold,  $P < 0.05$ ) with endothelial properties NO dependently. BM replacement by GFP- or  $\beta$ -galactosidase-overexpressing cells showed that Epo stimulated both differentiation of BM-derived EPCs and proliferation of resident ECs. BM-derived ECs increased 2.2- to 2.7-fold ( $P < 0.05$ ) in the Epo-induced neoendothelium, where the expression of Epo receptor was upregulated. Epo induced Akt/eNOS phosphorylation and NO synthesis on EPCs and exerted an antiapoptotic action on wire-injured arteries. In conclusion, Epo treatment inhibits the neointimal hyperplasia after arterial injury in an NO-dependent manner by acting on the injured vessels and mobilizing EPCs to the neo-endothelium. (*Circ Res.* 2006;98:1405-1413.)

**Key Words:** restenosis ■ endothelium ■ progenitor cells ■ erythropoietin

Endothelial cells (ECs) cover the luminal surface of blood vessels and maintain multiple vascular functions. Disruption of endothelial coverage causes a decrease in the production of vasculoprotective mediators such as nitric oxide (NO), leading to elevated vascular tonus, enhanced inflammation and medial smooth muscle cell proliferation. The resultant neointimal hyperplasia causes restenosis in various pathological conditions.<sup>1</sup>

Bone marrow (BM)-derived endothelial progenitor cells (EPCs) have been isolated from the mononuclear cell (MNC) population in peripheral blood (PB).<sup>2,3</sup> They have differentiated into ECs,<sup>2</sup> suggesting that they may have a potential to accelerate reendothelialization. Recently, transplantation of autologous PB EPCs to balloon-denuded arteries was reported to facilitate reendothelialization of the injured artery.<sup>4,5</sup> Intravenous transfusion of spleen-derived EPCs or EPCs overexpressing eNOS reduces neointimal formation after vascular injury.<sup>6,7</sup> Delivery of primary cultured PB MNCs to balloon-injured arteries leads to accelerated reendothelialization to promote endothelium-dependent vasoreactivity.<sup>8</sup>

Erythropoietin (Epo) stimulates the proliferation and differentiation of erythroid lineage progenitors. Mature ECs

express Epo receptors (EpoRs),<sup>9</sup> and Epo induces proangiogenic response in cultivated mature ECs, as evidenced by EC proliferation and migration<sup>10</sup> and the antiapoptotic effect on ECs<sup>11</sup> as well as NO production.<sup>12</sup> Epo increases circulating EPCs to stimulate neovascularization in vivo<sup>13</sup> or induces proangiogenic phenotype in cultured ECs<sup>14</sup> and also improves wound healing by angiogenesis in the genetically diabetic mouse.<sup>15</sup> This evidence leads to the hypothesis that Epo may provide an effective noninvasive strategy to enhance reendothelialization of injured vessels.

Several studies have shown that the exogenous administration of cytokines increases the number of circulating EPCs. For example, pretreatment with vascular endothelial growth factor (VEGF) was reported to double the number of circulating EPCs in humans,<sup>16,17</sup> and the administration of granulocyte colony-stimulating factor (G-CSF) recruited EPCs from BM.<sup>17</sup> Mobilization of the circulating EPCs by exogenous G-CSF facilitates reendothelialization and inhibits neointimal development.<sup>18</sup>

In this study, we evaluated the efficacy of short-term Epo treatment as a strategy for promoting reendothelialization followed by the inhibition of neointimal hyperplasia in

Original received November 28, 2005; revision received March 22, 2006; accepted April 18, 2006.

From the Departments of Cardiovascular Medicine (N.U., M.O., H.Y., A.M., S.M., K.T., T.N., T. Takahashi, T. Tatsumi, H.M.) and Pharmacology (K.M.), Kyoto Prefectural University of Medicine; and Department of Pathology (Y.A.), Kansai Medical University, Osaka, Japan.

Correspondence to Mitsuhiko Okigaki, MD, Department of Cardiovascular Medicine, Kyoto Prefectural University of Medicine, Kamigyo-ku, Kyoto 602-8566, Japan. E-mail okigakim@koto.kpu-m.ac.jp

© 2006 American Heart Association, Inc.

Circulation Research is available at <http://circres.ahajournals.org>

DOI: 10.1161/01.RES.0000224117.59417.f3

wire-injured arteries. Our results show that only 3-day treatment with Epo causes mobilization of circulating CD45<sup>dim</sup>/Flk-1<sup>+</sup> or Scd1<sup>+</sup>/Flk-1<sup>+</sup> EPCs and stimulates both differentiation of BM-derived EPCs on the endothelial layer and proliferation of resident ECs associated with endothelial EpoR-mediated activation of the Akt-eNOS pathway and SMC antiapoptotic effect, resulting in a marked inhibition of neointimal formation.

## Materials and Methods

### Vascular Injury, Epo Administration, and Morphometric Analysis

Transluminal arterial injury was performed in 8-week-old male C57BL/6 mice. A straight spring wire (0.25 mm in diameter) was inserted into the left femoral artery and placed there for 3 minutes. This wire injury was reported to cause a complete removal of endothelium.<sup>19</sup> Human Epo (Chugai, Tokyo) (1000 IU/kg body weight) or saline was injected intraperitoneally just after arterial injury and once daily for the following 2 days. Treatment with *N*<sup>G</sup>-nitro-L-arginine methyl ester (L-NAME) (3.7 mmol/L) or 2.25% L-arginine hydrochloride (106.8 mmol/L; Sigma) in the drinking water took place for 7 days before wire injury and continued for 14 days after wire injury.

The dose of Epo was determined based on the previous report.<sup>13</sup> The injured arteries were harvested at day 14 and fixed with 4% paraformaldehyde. Paraffin-embedded sections were stained with Elastica van Gieson. Three sections from each artery at 300- $\mu$ m intervals were analyzed using ImageJ 1.32j software (NIH). In other animals, Evans blue dye (5%; Sigma) was transfused to mice 10 minutes before euthanasia to identify the remaining denuded area 5 and 14 days after wire injury. After removal, arterial tissues were longitudinally opened and then placed on slide glasses to take pictures under microscope (MS5 Olympus). All animal procedures were approved by institutional guidelines. The collection of blood samples and the consent protocol for the volunteers was approved by institutional guidelines.

### Fluorescence-Activated Cell Sorting

PB (100  $\mu$ L) was collected 3 days after injury and incubated for 15 minutes with anti-mouse CD34-fluorescein isothiocyanate (FITC), Flk-1-PE, Scd1-FITC, CD45-PECy5 antibodies (BD Pharmingen). After erythrocyte lysis, cells were analyzed with FACS Caliber (Becton Dickinson). CD45<sup>dim</sup>/Flk-1<sup>+</sup> cells and Scd1<sup>+</sup>/Flk-1<sup>+</sup> cells were sorted with FACS Vantage to give a culture assay and RT-PCR analysis, respectively.

### Murine Cell Culture Assay

The sorted CD45<sup>dim</sup>/Flk-1<sup>+</sup> cells were cultured with EBM-2 medium supplemented with 5% FBS, EGM-2-MV-SingleQuots (Clonetics), and 10 ng/mL VEGF (Peprotech) on fibronectin-coated chamber slides (Becton Dickinson). Adherent cells were resceded after 4 days and maintained for 7 days. The culture cells were incubated with 2.4  $\mu$ L/mL Alexa Fluor 594-labeled acetylated LDL (acLDL) (Molecular Probes) for 120 minutes, fixed with 2% paraformaldehyde, and incubated with 10 ng/mL of BS-1-FITC (Sigma) for 1 hour, and double-fluorescent cells were counted as EPCs in 4 randomly selected fields under confocal microscopy (FLUOVIEW BX50; Olympus).

### Immunohistochemistry

Arteries were harvested on day 14 and fixed in 4% paraformaldehyde. Paraffin cross-sections were stained with antibodies against CD31 (sc-8306; Santa Cruz Biotechnology) and EpoR (sc-5624 or sc-697) followed by the avidin-biotin complex technique and diaminobenzidine substrate (Vector Laboratories). Sections were counterstained with hematoxylin. Frozen sections were stained with antibodies (GFP-Alexa Fluor 488, Molecular Probes; CD31-PE, BD

Pharmingen), followed by Alexa Fluor 633-conjugated anti-rabbit IgG secondary antibody (Molecular Probes), and then observed under the confocal microscopy. The number of fluorescent cells from 6 sections was evaluated statistically.

To detect apoptotic cells in situ, TdT-mediated dUTP-biotin nick end labeling (TUNEL) staining was performed for paraffin sections using the In-Situ Cell Death Detection Kit (Chemicon International Inc) and counterstained with methyl green.

### BM Transplantation

GFP transgenic mice were generously provided from Dr Okabe (Osaka University).<sup>20</sup> ROSA mice<sup>21</sup> were purchased from The Jackson Laboratory (Bar Harbor, Me). GFP- or  $\beta$ -galactosidase-overexpressing BM cells ( $5 \times 10^6$ ) were transfused to recipient mice 24 hours after 9 Gray irradiation. Six weeks after transplantation, they were subjected to vascular injury. Subsequently, at day 14 after injury, mice were examined.

### Human Cell Isolation and Culture

PB was obtained. PB MNCs from venous blood of healthy human volunteers were isolated by density-gradient centrifugation (Lymphoprep; Axis Shield). CD133<sup>+</sup> progenitor cells were purified from PB MNCs by positive selection with anti-CD133<sup>+</sup> microbeads respectively using magnetic cell sorter device (Miltenyi Biotec). The purity of sorted cells assessed by fluorescence-activated cell sorter (FACS) analysis was greater than 90%. The CD133<sup>+</sup> progenitor cells were cultured in EBM-2 medium supplemented with 5% FBS, EGM-2-MV-SingleQuots (Clonetics) a day before analysis, as described below. All cells were maintained at 37°C in a humidified incubator at 5% CO<sub>2</sub>. After serum starved in DMEM supplemented with 0.5% FBS for 12 hours, they were stimulated with 1.2IU/mL of Epo for 30 minutes and fixed. Immunofluorescence was performed by using antibodies against EpoR (sc-5624; Santa Cruz Biotechnology) with phosphorylated Akt and eNOS (Cell Signaling Technology). For double staining, we used Zenon rabbit IgG labeling kits (Molecular Probes) only when needed.

For measurement of the intracellular NO level, the cells were loaded with 4-amino-5-methylamino-2',7'-difluorofluorescein diacetate (DAF-FM DA) (10  $\mu$ mol/L; Daiichi Pure Chemicals, Tokyo, Japan) for 30 minutes at 37°C in the dark, washed twice with buffer, incubated for another 30 minutes, and then visualized under laser microscopy.

Fluorescent intensity was evaluated with Adobe Photoshop software.

### Measurement of NOx Concentration

NOx concentration in the serum was measured with a high-performance liquid chromatography (HPLC) Griess system, as previously described.<sup>22</sup>

### Statistics

Statistical analyses were performed with 1-way ANOVA followed by pair-wise contrasts using the Dunnett's test. Data are expressed as means  $\pm$  SE for continuous variables.  $P < 0.05$  was considered statistically significant.

## Results

### Epo Inhibits Neointimal Hyperplasia

A prominent, concentric neointima developed in the saline-treated vessels 14 days after injury, whereas neointimal formation was markedly reduced in the Epo-treated animals (Figure 1A). Morphometric analysis of serial sections (Figure 1B) showed a marked decrease (52%,  $n = 10$ ,  $P < 0.05$ ) in the neointimal area in the Epo-treated mice compared with the saline-injected group. The ratio of intima to medial area (I/M ratio) in the Epo-treated mice was significantly smaller (46%,  $n = 10$ ,  $P < 0.05$ ) than that in the saline-treated mice, whereas

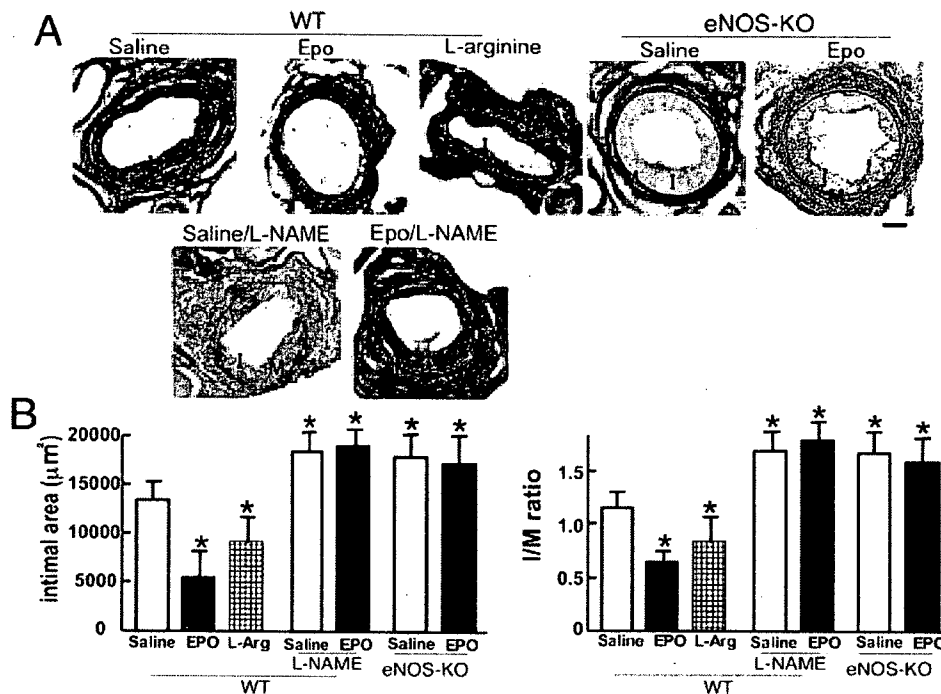


**Figure 1.** Epo-mediated inhibition of neointimal hyperplasia in NO-dependent manner. The wild-type or eNOS-null mice were subjected to the wire injury of femoral arteries and then treated with Epo or saline for the initial 3 days. Treatment with L-NAME (3.7 mmol/L) or 2.25% L-arginine hydrochloride (106.8 mmol/L) in the drinking water was started 7 days before wire injury and continued for 14 days until arterial sampling. A, Elastica van Gieson–stained sections on day 14. Scale bar=100 µm. I indicates intima; M, media. B, Quantification of the neointimal area and the I/M ratio averaged on 3 different sections of each artery (n=10 each). \*P<0.05 vs saline-treated wild-type mice.

medial thickness did not significantly differ between either group (data not shown).

As the involvement of NO in the neointimal hyperplasia has been reported,<sup>23</sup> we next examined the effect of L-NAME on the Epo-mediated inhibition. Seven-day pretreatment with L-NAME significantly aggravated the neointimal hyperplasia in the saline-treated control mice (31%, n=10, P<0.05), consistent with the previous reports using eNOS-null mice.<sup>24</sup> Interestingly, L-NAME completely abolished Epo-mediated inhibitory effect on the neointimal hyperplasia (I/M ratio; 1.61±0.38 versus 0.63±0.15 in the Epo-treated mice, P<0.05, n=10 each) (Figure 1A and 1B), suggesting the involvement of NO in Epo-mediated action. Furthermore, treatment with the NO donor L-arginine reduced the neointimal area to the level comparable to the Epo-treated mice (Figure 1A and 1B).

To confirm that the Epo-mediated inhibition of the neointimal formation is eNOS/NO dependent, we performed the arterial injury in the eNOS-null mice. The neointimal formation in the Epo-treated eNOS-null mice was aggravated (2.8-fold, n=7, P<0.005) compared with that of the Epo-treated wild-type mice, which was similar to the level in the Epo plus L-NAME–treated mice (2.9-fold, n=10, P<0.005) (Figure 1A and 1B).

The hemoglobin value was significantly higher after Epo treatment than that of the saline-treated controls (12.6±0.4 versus 14.0±0.1 g/dL at day 9, n=15, P<0.05). The number of white blood cells reached a peak on day 2 in both groups and was significantly higher in the Epo-treated mice

(18 600±2020 versus 10 200±1100 cells/µL of control, n=15, P<0.05). The platelet number was similar in both groups on days 2 and 9.

### Epo Promotes Reendothelialization

Evans blue dye was administered pre-mortem to stain the nonendothelialized areas 5 and 14 days after injury. Nonendothelialized lesions are marked by blue staining, whereas the reendothelialized area appears white (Figure 2A). At both time points, the reendothelialized area in the Epo-treated group was significantly larger than that in the saline-treated group (1.4- and 1.8-fold on day 5 and -14, n=6, respectively) (Figure 2A). Immunostaining with anti-CD31 antibody in transverse sections revealed that the proportion of CD31<sup>+</sup> length to total lumen surface was 1.4-fold greater in the Epo-treated mice (n=10, P<0.05) (Figure 2B), consistent with the result from Evans Blue dye experiment. Furthermore, the NO dependency of the Epo-promoted reendothelialization was evaluated. The CD31<sup>+</sup> endothelial area in the total lumen length in the Epo plus L-NAME–treated mice was 65% lower than that in the Epo-treated mice (n=10, P<0.01) and similar to the saline-treated control mice (Figure 2B).

### Epo Facilitates Mobilization of EPCs

CD45<sup>dim</sup> cells were gated from PB MNCs and subsequently analyzed for the expression of endothelial lineage markers, Flk-1 and CD34. Three-day Epo treatment mobilized the CD45<sup>dim</sup> cells into circulation (Figure 3A), and the ratio of CD45<sup>dim</sup>/Flk-1<sup>+</sup> cells to total PB MNCs increased to 7.4-fold (n=5 each, P<0.05) (Figure 3A, right). We further investi-



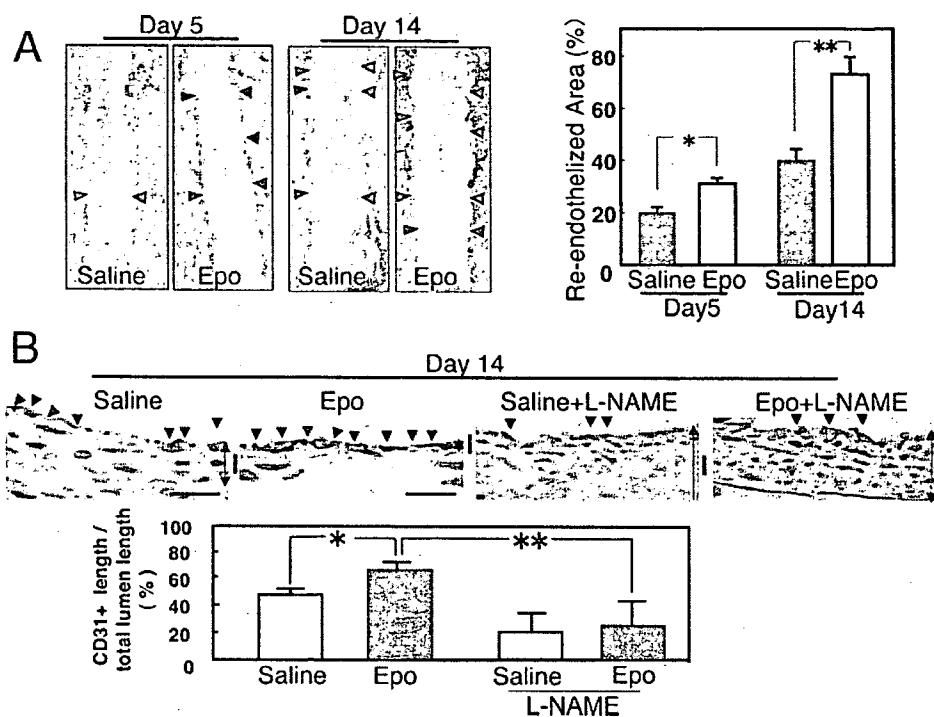


**Figure 2.** Epo facilitated reendothelialization after wire injury. **A**, Evans blue dye was injected 10 minutes before euthanasia on days 5 and 14. Nonendothelialized lesions are marked by blue staining, whereas the reendothelialized area appears white (arrowhead). Quantification of the reendothelialized areas was performed with computed morphometry ( $n=6$  each,  $*P<0.01$ ,  $**P=0.02$ ). **B**, Fourteen days after arterial injury with and without L-NAME pretreatment, the lesion was subjected to histological analysis. ECs were identified by immunostaining with anti-CD31 antibody in day-14 artery samples. Apparent CD31<sup>+</sup> area is indicated by arrowheads. The ratio of CD31<sup>+</sup> length to lumen perimeter in sections were evaluated and averaged on 5 different cross-sections from each artery ( $n=10$ ,  $*P<0.05$ ,  $**P<0.01$ ). I indicates intima.

gated the effect of L-NAME pretreatment on the Epo-mediated mobilization of EPCs using anti-Sca1 and anti-Flk-1 antibodies. The number of circulating Sca1<sup>+</sup>/Flk-1<sup>+</sup> cells in the control group was markedly increased than the basal level (2-fold,  $n=6$ ,  $P<0.05$ ), whereas in the L-NAME-treated group, the Epo-mediated mobilization was completely inhibited (Figure 3B).

To confirm the endothelial property of CD45<sup>dim</sup>/Flk-1<sup>+</sup> cells, we cultured them for 7 days in EGM medium with 10 ng/mL VEGF, and the EC-specific function was examined. Confocal microscopy demonstrated that  $93\pm 5\%$  of cultured CD45<sup>dim</sup>/Flk-1<sup>+</sup> cells were bound to FITC-conjugated BS-1 lectin and incorporated DiI-labeled acLDL, a commonly used identifier of endothelial lineage cells (Figure 3C). To evaluate the number of circulating EPCs, PB MNCs were isolated 3 days after Epo or saline treatment and cultured for 7 days. The relative numbers of BS-1 lectin<sup>+</sup>/acLDL<sup>+</sup> cells from Epo-treated mice were  $5.2\pm 0.5$ -fold higher ( $n=5$ ,  $P<0.02$ ) than that in the saline-injected control (Figure 3D).

### Antiapoptotic Effect on Medial SMC After Vascular Wire Injury

The procedure of wire injury of mouse femoral artery causes complete removal of endothelium, resulting in rapid apoptosis of medial SMCs that enhances neointimal hyperplasia.<sup>19,25</sup> Inhibition of this burst apoptosis is reported to be a preventive effect on neointimal hyperplasia.<sup>26</sup> Figure 3E shows that at 2

and 4 hours after injury, the number of TUNEL-positive apoptotic cells in the Epo-treated artery was significantly ( $P<0.05$ ) decreased to 25% and 39% of the saline-treated controls, respectively. L-NAME treatment did not affect the Epo-mediated protection of VSMC apoptosis. Considering that the endothelium was completely removed by wire injury and the expression of EpoR in the EC-denuded artery was detected by RT-PCR analysis (unpublished observation, 2006), these findings suggest that Epo directly affects the apoptosis of VSMCs after wire injury. Interestingly, at 6 hours after injury, the number of apoptotic cell in the Epo-treated mice was increased to the level similar to the saline-treated mice, suggesting that Epo treatment did not prevent, but shifted, the apoptosis of VSMCs after wire injury.

The biological effects of Epo in the injured artery may be attributable to Epo-induced increase in circulating NO pool produced by the remote endothelial cells. Plasma NO<sub>x</sub> concentrations at 1, 2, 4, and 6 hours and 1, 3, and 14 days after injury of the Epo-treated mice were similar to those of the control mice (day 1:  $54.3\pm 8.6$  versus  $57.2\pm 9.7$ ; day 3:  $58.6\pm 9.6$  versus  $55.3\pm 10.2$ ; day 14:  $59.6\pm 4.6$  versus  $60.8\pm 6.5$   $\mu\text{mol/L}$ ;  $n=7$  each). The expression levels for eNOS and EpoR in the lung and carotid artery at the same time points were comparable with the control mice when assessed by Western blotting and RT-PCR analysis, respectively (data not shown). These findings suggest that Epo-

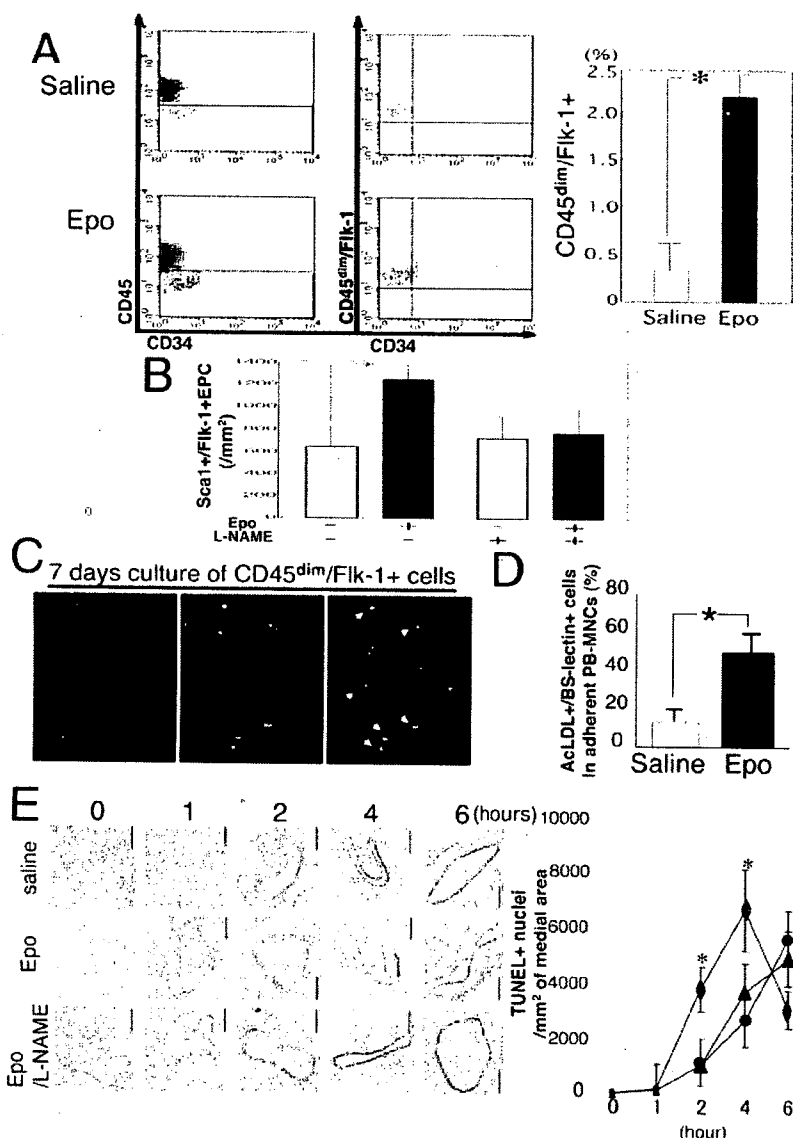


**Figure 3.** Identification of Epo-mobilized endothelial progenitor cells and antiapoptotic effect on medial SMCs. A, PB was collected 3 days after injury and subjected to FACS analysis. CD45<sup>dim</sup> cells were gated and subsequently analyzed for Flk-1 and CD34 expression. Right, Percentage of the CD45<sup>dim</sup>/Flk-1<sup>+</sup> cells in total PB MNCs was higher in the Epo-treated group (n=5, \*P<0.05). B, Evaluation of the number of circulating Sca1<sup>+</sup>/Flk-1<sup>+</sup> EPCs by FACS analysis. After 3 days of Epo treatment, the number of the circulating Sca1<sup>+</sup>/Flk-1<sup>+</sup> EPCs per millimeter squared of PB of the mice with or without 7 days of L-NAME pretreatment was evaluated (\*P<0.05, each n=4). C, Differentiation of CD45<sup>dim</sup>/Flk-1<sup>+</sup> cells into endothelial-lineage cells. PB MNCs were prepared from the 3-day Epo-treated mice, CD45<sup>dim</sup>/Flk-1<sup>+</sup> cells were sorted and primarily cultured for 7 days, and the endothelial properties were examined by the uptake of Dil-acLDL and binding to FITC-BS-1 lectin. Cells in the merged image (right, arrowheads) indicate BS-1 lectin<sup>+</sup>/acLDL<sup>+</sup> double-fluorescent cells. D, Total PB MNCs were primary cultured in endothelial medium for 7 days. The ratio of adherent cells with BS-1 lectin<sup>+</sup>/acLDL<sup>+</sup> EC-like property was shown (n=5, \*P<0.02). E, Time course of the apoptosis in the injured artery. Femoral arteries of mice treated with Epo, Epo plus L-NAME, or saline (n=5 each) were analyzed before and after 1, 2, 4, and 6 hours after wire injury. Apoptotic nuclei were detected as brown dots by TUNEL staining. Right, Semiquantification of TUNEL<sup>+</sup> nuclei in the medial area. Diamond, circle, and triangle indicate saline-, Epo-, and Epo plus L-NAME-treated mice, respectively. \*P<0.05 vs to Epo- and Epo plus L-NAME-treated mice.

mediated action unlikely results from the nonspecific increase in circulating NO pool.

### Analysis by BM Replacement Model

We further examined whether Epo actually induces the incorporation of marrow-derived EPCs into the regenerated endothelium by transplanting GFP-overexpressing or  $\beta$ -galactosidase BM cells to the BM-ablated background mice. Six weeks after transplantation, 96 $\pm$ 2% and 94 $\pm$ 3% of PB MNCs were replaced, respectively (n=5 each; FACS data not shown). The mice that received vascular injury were examined on day 14. GFP<sup>+</sup> and  $\beta$ -Gal<sup>+</sup> cells were patchily detected in the endothelial layer, and double-fluorescence immunohistochemistry (Figure 4A and 4B) disclosed a significant increase in the GFP<sup>+</sup>/CD31<sup>+</sup> and  $\beta$ -Gal<sup>+</sup>/CD31<sup>+</sup> lesions (2.7- and 2.2-fold, respectively, P<0.05) in Epo-treated mice compared with the saline-treated mice (Figure 4A and 4B). The ratio of Epo-induced GFP<sup>+</sup> area in total CD31<sup>+</sup> regenerated endothelium was 31 $\pm$ 0.3% (n=5) (Figure 4A), suggesting that Epo-mediated reendothelialization is

composed of differentiation of BM-derived EPCs as well as facilitated proliferation of resident ECs. In addition, the numbers of BM-derived macrophages (GFP<sup>+</sup>/MOMA2<sup>+</sup>) and vascular smooth muscle cells (GFP<sup>+</sup>/ $\alpha$ SMA<sup>+</sup>) in the neointima of the Epo-treated mice were much lower than those of the control group (Figure 4A). GFP<sup>+</sup>/CD3<sup>+</sup> or GFP<sup>+</sup>/B220<sup>+</sup> cells were barely detectable in the neointima of both groups (data not shown).

### Expression of EpoR in Epo-Treated Injured Artery

We investigated whether Epo-mobilized EPCs actually express the specific receptor for Epo (EpoR). EpoR-positive cells (brown staining, arrowheads in Figure 5A) were apparently localized on the regenerated endothelium in the Epo-treated arteries, whereas the expression of EpoR in the saline-treated injured or uninjured arteries was barely detectable.

The immunofluorescence study using anti-EpoR, anti-CD31, anti-CD45, and anti- $\alpha$ SM-actin ( $\alpha$ SMA) antibodies revealed that CD31<sup>+</sup> endothelial cells in Epo-treated arteries coexpressed EpoR on the endothelial layer, whereas neither

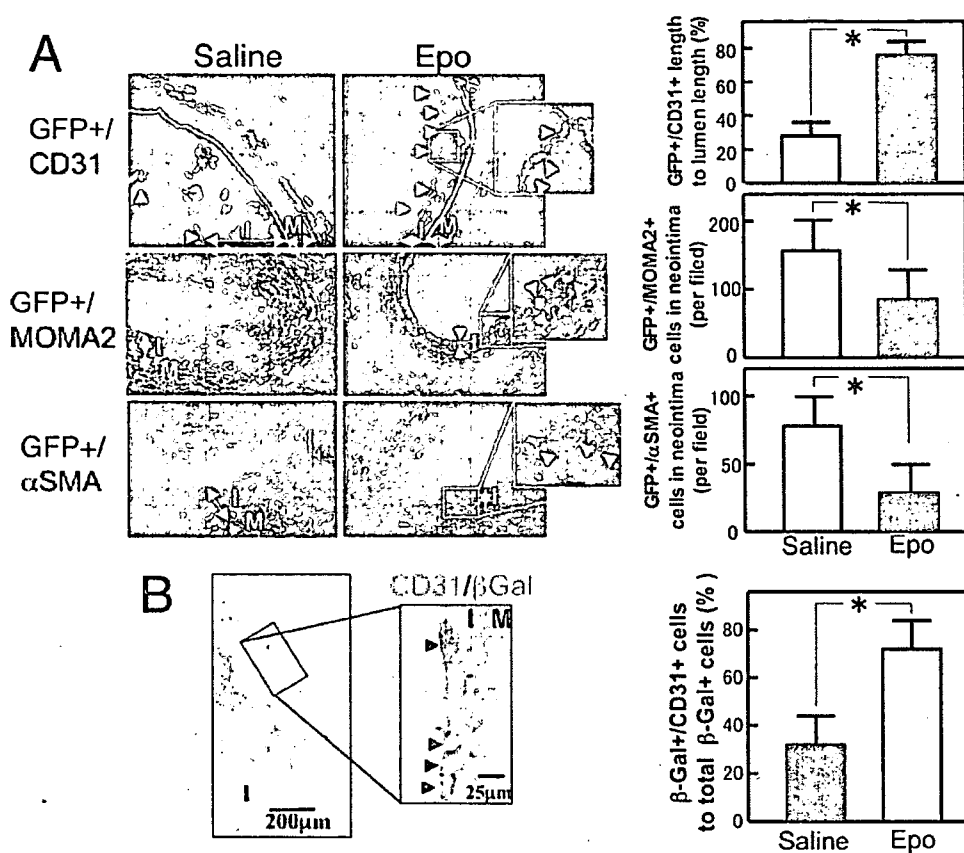


**Figure 4.** Incorporation of BM-derived cells into regenerated endothelium. A, BM cells from donor GFP-overexpressing mice were transfused to the irradiated recipient mice and subject to vascular injury. The day-14 samples were immunostained with antibodies against CD31, MOMA2,  $\alpha$ SMA, and GFP. The localizations of double-fluorescent cells, including GFP<sup>+</sup>/CD31<sup>+</sup>, GFP<sup>+</sup>/MOMA2, and GFP<sup>+</sup>/ $\alpha$ SMA cells, are shown as yellow dots in the merged image (arrowheads, bar=20  $\mu$ m). Semiquantitative analysis of the double-fluorescent cell area per section is shown relative to the total lumen length or the number in the neointima (n=5 each, \* $P$ <0.02). B, BM cells from donor  $\beta$ -Gal-overexpressing mice were transfused to the irradiated recipient mice and subjected to vascular injury.  $\beta$ -Gal-expressing cells (blue) and CD31<sup>+</sup> cells (brown) were observed in the day-14 samples.  $\beta$ -Gal<sup>+</sup>/CD31<sup>+</sup> double-stained cells are indicated by arrowheads, and the relative ratio to total  $\beta$ -Gal<sup>+</sup> cells is shown (n=5 in each group, \* $P$ <0.05).

CD45<sup>+</sup> cells nor  $\alpha$ SMA<sup>+</sup> cells expressed EpoR (Figure 5B). We also confirmed the expression of EpoR in the BM-derived EC-like cells mobilized by Epo using the mice repopulated with GFP<sup>+</sup> BM cells (Figure 5C). Abundant GFP<sup>+</sup>/EpoR<sup>+</sup> cells were detected on the luminal surface in the Epo-treated injured artery, and the distribution was 2.5-fold greater than that in the saline-treated mice ( $P$ <0.05, Figure 5D).

#### Epo Activates Akt-eNOS Pathways and NO Production in EPCs

To investigate whether PB and BM EPCs express EpoR, Scal<sup>+</sup>/Flk-1<sup>+</sup> EPCs were isolated from PB and BM by FACS and subjected to RT-PCR analysis. The DNA fragment corresponding to EpoR was amplified in the predicted size (Figure 6A). We further studied whether Scal<sup>+</sup>/Flk-1<sup>+</sup> EPCs have the ability to activate the EpoR/Akt/eNOS pathway in response to Epo treatment. Because the PB volume obtained from the mice is too little to get the sufficient number of endothelial-lineage cells attaching on the plate, and also the attaching mice-derived cells are less spreading and less proliferative compared with the human cells, we used the human PB EPCs. The CD133<sup>+</sup> EPCs were isolated from human PB by magnetic-associated cell sorting and primarily

cultured. To study the stimulatory effect of Epo on the downstream pathway, after 12-hour serum starvation (0.5% serum), CD133<sup>+</sup> EPCs were treated with 1.2 IU/mL Epo for 30 minutes. Double staining using anti-EpoR with anti-phosphorylated Akt or anti-phosphorylated eNOS antibodies showed that Epo markedly induced Akt-eNOS phosphorylation in EpoR-positive EPCs (Figure 6B).

We further measured the intracellular NO level with DAF-FM DA (10  $\mu$ mol/L). NO was visualized as a green dot under laser microscopy (Figure 6C). Epo stimulation upregulated NO level to 1.7-fold higher than the untreated control level ( $P$ <0.05), whereas addition of L-NAME completely abolished this increase.

#### Discussion

The balloon-mediated injury of endothelial integrity stimulates a regeneration of the EC monolayer, but this regenerative process is slow and cannot prevent the early proliferative events leading to the onset of a neointimal lesion. A novel approach that promotes early reendothelialization is required to potentiate this natural regenerative process. In this study, we examined whether Epo treatment is a feasible strategy to cause reendothelialization of wire-injured vessels. Our results

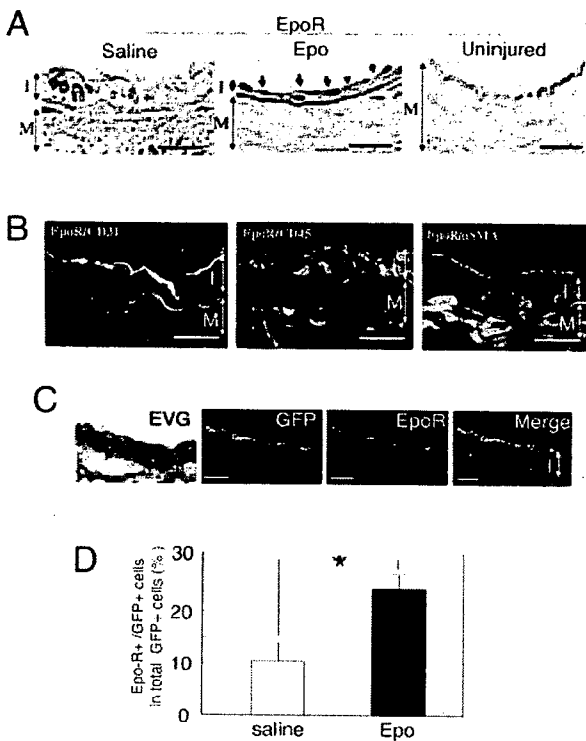


**Figure 5.** Localization and characterization of EpoR-expressing cells in neointima. A, Immunohistochemistry for EpoR showing the abundant localization of EpoR-expressing cells (brown, arrowheads) in the Epo-treated artery (day-14 sample) compared with saline-treated control and uninjured artery (bar=50  $\mu$ m). B, Double-immunofluorescent images for EpoR (red) and CD31 (green, left), CD45 (green, middle), or  $\alpha$ SMA (green, right) (bar=20  $\mu$ m) showing coexpression of EpoR in CD31<sup>+</sup> cells. C, Localization of BM-derived EpoR-expressing cells in Epo-treated mice repopulated with GFP-overexpressing BM cells. Elastica van Gieson-stained sections (left) and immunofluorescent images for GFP (green) and EpoR (red) showing the localization of BM-derived EpoR<sup>+</sup> cells (yellow in merge image) along neointimal surface (bar=50  $\mu$ m). D, Relative percentage of BM-derived EpoR-expressing cells in total BM-derived GFP<sup>+</sup> cells in the neointima (n=5 each, \*P<0.05). I indicates intima; M, media.

demonstrated that the 3-day treatment of Epo increases the circulating Sca-1<sup>+</sup>/Flk-1<sup>+</sup> EPCs expressing an EpoR and that the mobilized EPCs contribute to the reendothelialization, leading to the inhibition of neointimal hyperplasia in an NO-dependent manner. Furthermore, we found that EpoR expression is upregulated in the Epo-induced neoendothelium and that the Epo/EpoR system causes the activation of the Akt-eNOS pathway on the EPCs and inhibits the apoptosis of medial SMCs.

EPCs can be harvested from PB, and intravenous transplantation of EPCs into EC-denuded vessels potentiates the recovery of endothelial integrity that causes the inhibition of neointimal hyperplasia,<sup>4,8</sup> although cell transplantation protocols, such as the ex vivo expansion of EPCs, are technically challenging. G-CSF-induced EPCs were shown to enhance the repair of injured arteries and prevent intimal hyperplasia.<sup>18</sup> However, it appears that the safety and feasibility of G-CSF treatment focusing on the induction of vascular occlusion in atherosclerotic lesions has not yet been estab-

lished. In 12 intractable angina patients, the administration of G-CSF was associated with 2 cases of acute myocardial infarction and 1 case of cardiac death.<sup>27</sup> There are articles reporting the induction of acute myocardial infarction and cerebral infarction in G-CSF-treated BM transplantation patients.<sup>28,29</sup> Differentiation of G-CSF-mobilized progenitor cells into VSMC within the stented segment, induction of angiogenesis within the atherosclerotic lesion, and aggregation of mobilized inflammatory cells within the plaque may be plausible explanations.

This study showed that short-term (3-day) treatment with Epo after EC-denuded injury leads to accelerated reendothelialization and marked inhibition of neointimal formation. Figure 2A demonstrates that the ratio of reendothelialization by Epo and saline treatment is 73% and 41% on the total lumen area, respectively, whereas the coverage by CD31<sup>+</sup> marrow-derived cells on the reendothelialized lumen area is 75% and 32%, respectively (Figure 4B), indicating that 55% of Epo-mediated reendothelialized area is derived from marrow cells, and, in the saline-treated control, 13% of reendothelialized area is marrow-derived cells. Considering that Epo-mediated EPC mobilization (Figure 3) and reendothelialization (Figure 2) are NO dependent, it is suggested that EPC release via Epo and the endothelial differentiation in the repair process is partly involved in the observed reduction of neointima. Although the mobilization of EPC might be considered unfavorable for tumor growth, multiple clinical trials have recommended the use of Epo in chemotherapy-associated anemia or for longer survival among patients with multiple myeloma.<sup>30</sup> Thus, the safety and feasibility of Epo treatment has been established. Although it was a concern that erythropoiesis may increase the risk of thrombosis because of an elevation in blood viscosity or cause hypertension resulting from the induction of the vasoconstricting hormone endothelin-1,<sup>31</sup> thrombosis formation at the injured lesion in the Epo-treated group was similar to the saline-injected group, and blood pressure did not increase after short-term Epo-treatment (unpublished observation, 2005). Moreover, Epo was reported to attenuate cytokine production and inflammation in tissue ischemia by targeting cell apoptosis<sup>32</sup> or to induce cellular protection by activating Epo-EpoR signals involving Akt pathways,<sup>33</sup> consistent with the present result (Figure 6). These antiinflammatory and antiapoptotic cytoprotection actions associated with endothelial EpoR-mediated Akt/NO signaling may also contribute to the preventive effect of Epo on the neointimal hyperplasia.

EPC-like cells were reportedly derived from more differentiated CD34<sup>+</sup> or immature CD133<sup>+</sup> hematopoietic stem cells, as well as from PB MNCs or CD14<sup>+</sup> monocytes.<sup>2,8,16</sup> These EPC-like cells lose CD45 hematopoietic markers and express endothelial markers. Our present study clearly showed that CD45<sup>dim</sup>/Flk-1<sup>+</sup> or Sca1<sup>+</sup>/Flk-1<sup>+</sup> EPCs were mobilized by Epo, had a functional EC-like property in vitro, and contributed to endothelial regeneration after wire-mediated injury, suggesting this cell type is an EPC-like cell responsible for Epo-induced vascular repair. Thus, Epo treatment may be a novel strategy to inhibit the neointimal hyperplasia by directly acting on the injured vessels as well as mobilizing EPCs to the neoendothelium.